Advanced Review

Subsystem density-functional theory

Christoph R. Jacob[1]* and Johannes Neugebauer[2]*

Subsystem density-functional theory (subsystem DFT) has developed into a powerful alternative to Kohn–Sham DFT for quantum chemical calculations of complex systems. It exploits the idea of representing the total electron density as a sum of subsystem densities. The optimum total density is found by minimizing the total energy with respect to each of the subsystem densities, which breaks down the electronic-structure problem into effective subsystem problems. This enables calculations on large molecular aggregates and even (bio-)polymers without system-specific parameterizations. We provide a concise review of the underlying theory, typical approximations, and embedding approaches related to subsystem DFT such as frozen-density embedding (FDE). Moreover, we discuss extensions and applications of subsystem DFT and FDE to molecular property calculations, excited states, and wave function in DFT embedding methods. Furthermore, we outline recent developments for reconstruction techniques of embedding potentials arising in subsystem DFT, and for using subsystem DFT to incorporate constraints into DFT calculations.

How to cite this article:
WIREs Comput Mol Sci 2014, 4:325–362. doi: 10.1002/wcms.1175

INTRODUCTION

The increasing accuracy of approximate electronic-structure methods and the availability of ever-more powerful computational resources has led to a widespread application of quantum-chemical methods to molecular systems of ever larger complexity and size.[1–3] More and more detailed analyses of effects of environments surrounding reaction centers, interactions between functional components, and potentially active ingredients in large chemical systems are carried out.[4–6] This has triggered an immense activity in the quantum chemistry community to develop methods specifically suited for treating large systems (see, e.g., Refs 1, 5, 7–10).

Conventional wave function–based quantum chemical methods face the so-called "curse-of-dimension" problem, which is related to their unfavorable scaling with the system size.[11,12] Ideally, one would hope that a linear scaling of computational effort with the number of atoms in a chemical system can be achieved, whereas the (potentially exact) full configuration interaction method shows a factorial scaling with system size. A natural way of reducing the scaling behavior is to partition the total system into fragments or subsystems[13] and to treat each subsystem individually. This idea forms, in one way or another, the basis for most low-order scaling quantum chemical methods, usually at the expense of more or less drastic approximations.

One strategy in this field is subsystem density functional theory (subsystem DFT), which achieves a partitioning into subsystems on the basis of the electron density $\rho(\mathbf{r})$.[14–16] Subsystem DFT has several important advantages compared to other fragment-based approaches, although it is not yet at a stage where it can be applied to arbitrary partitionings in a black-box manner. The advantages are in particular: (i) Subsystem DFT is an alternative to other density-functional theory methods, most notably

The authors have declared no conflicts of interest in relation to this article.

*Correspondence to: christoph.jacob@kit.edu, j.neugebauer@uni-muenster.de

[1]Center for Functional Nanostructures and Institute of Physical Chemistry, Karlsruhe Institute of Technology (KIT), Karlsruhe, Germany

[2]Theoretische Organische Chemie, Organisch-Chemisches Institut, Westfälische Wilhelms-Universität Münster, Münster, Germany

DOI: 10.1002/wcms.1175

the Kohn–Sham (KS) method and thus potentially exact in the limit of exact energy functionals. (ii) An embedding potential naturally arises in the context of subsystem DFT, which describes the effect of all other subsystems onto the one for which the electronic structure shall be determined. This embedding potential carries a dependence only on the electron density of the other subsystems, but not on their wave functions or other quantities. This forms the basis of the so-called frozen-density embedding (FDE) theory.[17] (iii) Subsystem DFT achieves a partitioning in terms of the measurable real-space quantity $\rho(\mathbf{r})$, and thus also leads to a very intuitive partitioning in line with chemical concepts.

In the following, we will first discuss fundamental theoretical aspects of subsystem DFT and FDE, followed by a review of the properties of the embedding potential arising in the subsystem DFT working equations. Besides other aspects, the following section deals with the quality of electron densities obtained from subsystem DFT, which is determined by the quality of the potential, and the reconstruction of exact embedding potentials. Afterward, we concentrate on interaction energies calculated from subsystem DFT, which also includes the interaction between "quasi-diabatic" potential energies constructed from approximate subsystem DFT methods. We summarize and review the state-of-the-art in property and spectra calculations on the basis of subsystem DFT. We continue with a presentation of mixed wave function/DFT subsystem methods, before we conclude on the current status of this field.

FUNDAMENTALS OF SUBSYSTEM DFT AND RELATED METHODS

Kohn–Sham DFT

The total energy expression in Kohn–Sham DFT is usually written as (using Hartree atomic units and including the nucleus–nucleus terms),[18,19]

$$E[\rho] = T_s[\rho] + V_{\mathrm{nuc}}[\rho] + J[\rho] + E_{\mathrm{xc}}[\rho] + V_{\mathrm{nn}} \tag{1}$$

where V_{nuc} is the electron–nucleus interaction,

$$V_{\mathrm{nuc}}[\rho] = \int \rho(\mathbf{r}) v_{\mathrm{nuc}}(\mathbf{r}) \mathrm{d}\mathbf{r} \tag{2}$$

$$v_{\mathrm{nuc}}(\mathbf{r}) = -\sum_I \frac{Z_I}{|\mathbf{R}_I - \mathbf{r}|}, \tag{3}$$

V_{nn} is the nucleus–nucleus repulsion,

$$V_{\mathrm{nn}} = \sum_{I,J} \frac{Z_I Z_J}{|\mathbf{R}_I - \mathbf{R}_J|}, \tag{4}$$

which is constant for a fixed geometric structure, $J[\rho]$ is the electron–electron Coulomb repulsion,

$$J[\rho] = \frac{1}{2} \int \frac{\rho(\mathbf{r})\rho(\mathbf{r}')}{|\mathbf{r} - \mathbf{r}'|} \mathrm{d}\mathbf{r}\mathrm{d}\mathbf{r}' \tag{5}$$

$T_s[\rho]$ is the (noninteracting) kinetic energy of the Kohn–Sham reference system, and $E_{\mathrm{xc}}[\rho]$ is the exchange–correlation energy functional defined as

$$E_{\mathrm{xc}}[\rho] = (V_{\mathrm{ee}}[\rho] - J[\rho]) + (T[\rho] - T_s[\rho]). \tag{6}$$

$E_{\mathrm{xc}}[\rho]$ has to be approximated in KS-DFT calculations, as its precise analytic form is unknown. In the above equation, $V_{\mathrm{ee}}[\rho]$ is the full electron–electron interaction energy, and $T[\rho]$ is the true kinetic energy of the n-electron system. Both are not known explicitly as functionals of the electron density, but can be expressed through the n-electron wave function Ψ, This n-electron wave function Ψ is determined by the electron density ρ. In Levy's constrained search formulation of DFT,[20,21] Ψ can be obtained from the minimization,

$$\begin{aligned} F_{HK}[\rho] &= \min_{\Psi \to \rho} \langle \Psi | \hat{T} + \hat{V}_{\mathrm{ee}} | \Psi \rangle \\ &= \min_{\Psi \to \rho} \left\langle \Psi \left| \sum_i^n -\nabla_i^2/2 + \sum_{i>j}^n 1/r_{ij} \right| \Psi \right\rangle, \end{aligned} \tag{7}$$

where the constrained search includes all wave functions that correspond to the electron density ρ. With this wave function available as a functional of the electron density, the full electron–electron interaction energy and the true kinetic energy can be calculated as

$$V_{\mathrm{ee}}[\rho] = \left\langle \Psi[\rho] \left| \sum_{ij}^n 1/r_{ij} \right| \Psi[\rho] \right\rangle \tag{8}$$

$$T[\rho] = \left\langle \Psi[\rho] \left| \sum_i^n -\nabla_i^2/2 \right| \Psi[\rho] \right\rangle. \tag{9}$$

Also $T_s[\rho]$ is unknown as an explicit density functional in general, but can be defined as

$$\begin{aligned} T_s[\rho] &= \min_{\Psi_s \to \rho} \left\langle \Psi_s \left| \sum_i^n -\nabla_i^2/2 \right| \Psi_s \right\rangle \\ &= \min_{\{\psi_i\} \to \rho} \sum_i^n \left\langle \psi_i \left| -\nabla^2/2 \right| \psi_i \right\rangle. \end{aligned} \tag{10}$$

Here, the constrained search is performed over all wave functions Ψ_s of a reference system of noninteracting electrons with the density ρ (i.e, single Slater determinant wave functions). The Kohn–Sham orbitals ψ_i are the orthonormal orbitals appearing in

this Slater determinant. In terms of these KS orbitals, the electron density is given by

$$\rho(\mathbf{r}) = \sum_{i}^{n} |\psi_i(\mathbf{r})|^2. \tag{11}$$

In the following, we will denote $T_s[\rho]$ as an explicit functional of the Kohn–Sham orbitals,

$$T_s[\{\psi_i\}] = \sum_{i}^{n} \langle \psi_i \,| -\nabla^2/2 |\, \psi_i \rangle. \tag{12}$$

The Kohn–Sham energy expression should thus better be written as,

$$E[\{\psi_i\}] = T_s[\{\psi_i\}] + V_{\text{nuc}}[\rho] + J[\rho] + E_{\text{xc}}[\rho] + V_{\text{nn}}. \tag{13}$$

Minimization of $E[\{\psi_i\}]$ in Kohn–Sham DFT with respect to the Kohn–Sham orbitals, under the constraint that these remain orthonormalized, leads to effective single-particle Schrödinger Equations for the Kohn–Sham orbitals, the so-called Kohn–Sham equations,

$$\left(-\frac{\nabla^2}{2} + v_{\text{eff}}[\rho](\mathbf{r})\right)\psi_i(\mathbf{r}) = \epsilon_i \psi_i(\mathbf{r}), \qquad i = 1, \ldots, n \tag{14}$$

where the effective Kohn–Sham potential is given by

$$v_{\text{eff}}[\rho](\mathbf{r}) = v_{\text{nuc}}(\mathbf{r}) + v_{\text{Coul}}[\rho](\mathbf{r}) + v_{\text{xc}}[\rho](\mathbf{r}), \tag{15}$$

with the electronic Coulomb and exchange–correlation potentials

$$v_{\text{Coul}}[\rho](\mathbf{r}) = \int \frac{\rho(\mathbf{r}')}{|\mathbf{r} - \mathbf{r}'|} \mathrm{d}\mathbf{r}' \tag{16}$$

$$v_{\text{xc}}[\rho](\mathbf{r}) = \frac{\delta E_{\text{xc}}[\rho]}{\delta \rho(\mathbf{r})}. \tag{17}$$

Subsystem DFT

Starting point for subsystem DFT[14–16] (for earlier reviews, see Refs 22 and 23, and the overview over the field given in Ref 24) is a partitioning of the electron density,

$$\rho(\mathbf{r}) = \rho_{\text{tot}}(\mathbf{r}) = \sum_{I} \rho_I(\mathbf{r}). \tag{18}$$

The subsystem densities ρ_I are then each expressed through systems of noninteracting particles, that is, through orbitals of the corresponding subsystem,

$$\rho_I(\mathbf{r}) = \sum_{i_I}^{n_I} |\psi_{i_I}(\mathbf{r})|^2, \tag{19}$$

where the sum runs over all n_I occupied orbitals in subsystem I. The essential difference between this ansatz and the Kohn–Sham approach is that we are no longer able to use $T_s[\{\psi_i(\mathbf{r})\}]$, the noninteracting kinetic energy of the total system, since this would require knowledge of the orbitals of the total system. Instead, we can define subsystem kinetic energies,

$$T_s[\{\psi_{i_I}\}] = \sum_{i_I}^{n_I} \langle \psi_{i_I} \,| -\nabla^2/2 |\, \psi_{i_I} \rangle. \tag{20}$$

As a rough approximation to the total T_s, one could use the sum of all subsystem kinetic energies,

$$T_s[\{\psi_i\}] \approx \sum_{I} T_s[\{\psi_{i_I}\}]. \tag{21}$$

The expression can be formally made exact again by introducing a nonadditive kinetic energy term,

$$T_s^{\text{nad}}[\{\psi_i\}, \{\{\psi_{i_I}\}\}] = T_s[\{\psi_i\}] - \sum_{I} T_s[\{\psi_{i_I}\}], \tag{22}$$

or, expressed as a density functional,

$$T_s^{\text{nad}}[\{\rho_I\}] = T_s[\rho_{\text{tot}}] - \sum_{I} T_s[\rho_I], \tag{23}$$

where the subsystem kinetic energies are defined in analogy to Eq. (10).

The subsystem-DFT energy expression is thus

$$E[\{\psi_{i_I}\}] = \sum_{I} T_s[\{\psi_{i_I}\}] + V_{\text{nuc}}[\rho] + J[\rho] + E_{\text{xc}}[\rho] + T_s^{\text{nad}}[\{\rho_I\}] + V_{mn}. \tag{24}$$

Minimization of this energy expression with respect to the Kohn–Sham-like orbitals $\{\psi_{i_K}\}$ of subsystem K, under the constraint that these subsystem orbitals are orthonormal and the electron densities of the other subsystems are fixed, leads to Kohn–Sham-like equations for this subsystem. These are known as the Kohn–Sham equations with constrained electron density (KSCED[17,22]),

$$\left(-\frac{\nabla^2}{2} + v_{\text{eff}}^{(K)}[\rho_K](\mathbf{r}) + v_{\text{emb}}^{(K)}[\rho_K, \rho_{\text{tot}}](\mathbf{r})\right)\psi_{i_K}(\mathbf{r}) = \epsilon_{i_K}\psi_{i_K}(\mathbf{r}), \qquad i = 1, \ldots, n. \tag{25}$$

Here, $v_{\text{eff}}^{(K)}[\rho_K](\mathbf{r})$ has to be understood as

$$v_{\text{eff}}^{(K)}[\rho_K](\mathbf{r}) = v_{\text{nuc}}^{(K)}(\mathbf{r}) + v_{\text{Coul}}[\rho_K](\mathbf{r}) + v_{\text{xc}}[\rho_K](\mathbf{r}), \tag{26}$$

and contains all the terms that would also be present in a Kohn–Sham DFT calculation for the isolated subsystem K. In particular, the nuclear potential $v_{\text{nuc}}^{(K)}(\mathbf{r})$ considers all nuclei assigned to subsystem K.

The additional embedding potential for system K is given by

$$v_{\text{emb}}^{(K)}[\rho_K, \rho_{\text{tot}}](\mathbf{r}) = \sum_{I, I\neq K} v_{\text{nuc}}^{(I)}(\mathbf{r}) + v_{\text{Coul}}[\rho_{\text{tot}} - \rho_K](\mathbf{r}) + v_{\text{xc}}^{\text{nad}}[\rho_K, \rho_{\text{tot}}](\mathbf{r}) + v_{\text{kin}}^{\text{nad}}[\rho_K, \rho_{\text{tot}}](\mathbf{r}). \quad (27)$$

Note that, in addition to the densities ρ_K and ρ_{tot}, this embedding potential also depends on the nuclear potentials $v_{\text{nuc}}^{(I)}$ of the other subsystems. It is thus subsystem specific, which is indicated by the superscript $^{(K)}$. The nonadditive kinetic energy introduces a corresponding contribution to the embedding potential, which is given by

$$v_{\text{kin}}^{\text{nad}}[\rho_K, \rho_{\text{tot}}](\mathbf{r}) = \frac{\delta T_s^{\text{nad}}[\{\rho_I\}]}{\delta\rho_K(\mathbf{r})} = \frac{\delta T_s[\rho_{\text{tot}}]}{\delta\rho_{\text{tot}}(\mathbf{r})} - \frac{\delta T_s[\rho_K]}{\delta\rho_K(\mathbf{r})}. \quad (28)$$

Here and in the following, expressions like $\frac{\delta T_s[\rho_K]}{\delta\rho_K(\mathbf{r})}$ have to be understood as $\frac{\delta T_s[\rho]}{\delta\rho(\mathbf{r})}\Big|_{\rho(\mathbf{r})=\rho_K(\mathbf{r})}$, that is, the functional derivative of $T_s[\rho]$, evaluated for the density $\rho_K(\mathbf{r})$. In the following, we will refer to the contribution $v_{\text{kin}}^{\text{nad}}[\rho_K, \rho_{\text{tot}}]$ as *nonadditive kinetic potential*. A similar nonadditive contribution arises from the exchange–correlation functional, which is given by

$$v_{\text{xc}}^{\text{nad}}[\rho_K, \rho_{\text{tot}}](\mathbf{r}) = v_{\text{xc}}[\rho_{\text{tot}}](\mathbf{r}) - v_{\text{xc}}[\rho_K](\mathbf{r}) = \frac{\delta E_{\text{xc}}[\rho_{\text{tot}}]}{\delta\rho_{\text{tot}}(\mathbf{r})} - \frac{\delta E_{\text{xc}}[\rho_K]}{\delta\rho_K(\mathbf{r})}. \quad (29)$$

The essential ingredients of subsystem DFT can already be found in the work of Senatore and Subbaswamy,[14,15] whereas a more formal derivation has been given by Cortona.[16] Non-selfconsistent predecessor methods can be traced back to the work by Gordon and Kim,[25,26] and the density partitioning idea is already expressed by Gombas.[27]

Finally, we would like to note that subsystem DFT can be extended within the generalized Kohn–Sham context to allow for hybrid exchange–correlation energy functionals and the corresponding nonlocal potentials.[28–30] Usually, however, simple semilocal approximations are then still employed for the nonadditive part of the exchange–correlation potential.

Frozen-Density Embedding Theory

While in a conventional KS-DFT calculation, the whole system is treated as one entity (see Fig. 1(a)), in subsystem DFT it is split into subsystems, which are each treated on an equal footing (see Fig. 1(b)). Starting from a subsystem description, one can set up embedding methods in which one particular subsystem is considered to be embedded in an effective environmental potential. This potential can be derived from a given environmental density. This so-called frozen-density embedding (FDE) theory was first proposed in a seminal paper by Wesołowski and Warshel,[17] and—being a formally exact theory—provides the reference point for any approximate embedding method used in practical applications. In FDE, one partitions the electron density into an active subsystem and a frozen environment part,

$$\rho(\mathbf{r}) = \rho_A(\mathbf{r}) + \rho_B(\mathbf{r}) \quad (30)$$

$$= \rho_{\text{active}}(\mathbf{r}) + \rho_{\text{environment}}(\mathbf{r}). \quad (31)$$

The properties of the active system (system A) can then be determined in the presence of an environment with density $\rho_B(\mathbf{r})$, which is approximated at the beginning of the calculation and subsequently kept fixed. Note that this frozen environment could be further decomposed into subsystems. In this way, the environment density is *defined* based on a reasonable starting point, usually the density of the environment without the active system. One then calculates the density of the active subsystem in the presence of this (approximate) environment density (see Fig. 1(c)) by employing the embedding potential of Eq. (27).

Some fundamental aspects of FDE, which have been controversially discussed in the recent literature, deserve special attention. One point of view can be expressed as follows: If we define the target density to be produced by the embedding potential as the difference between the exact density and the frozen environment density,

$$\rho_A^{\text{target}}(\mathbf{r}) := \rho_{\text{exact}}(\mathbf{r}) - \rho_B^{\text{frozen}}(\mathbf{r}), \quad (32)$$

and if this target density is v_s-representable, that is, if it can be represented as the density obtained from the ground state of a reference system of noninteracting electrons,[18,22] then an energy minimization of the total energy with respect to ρ_A will lead to the correct total electron density and energy in the limit of exact functionals. An important necessary condition for this v_s-representability is that $\rho_A^{\text{target}}(\mathbf{r}) \geq 0$ everywhere in space. In practice, it turns out that this condition is rather difficult to fulfill. This can be investigated by accepting the error introduced by the approximate exchange–correlation functional, both in the KS- and the FDE calculation, and replacing the "exact" density in Eq. (32) by the result of a Kohn–Sham DFT calculation. As shown in Ref 31, the target density usually shows negative areas if ρ_B^{frozen} is obtained from

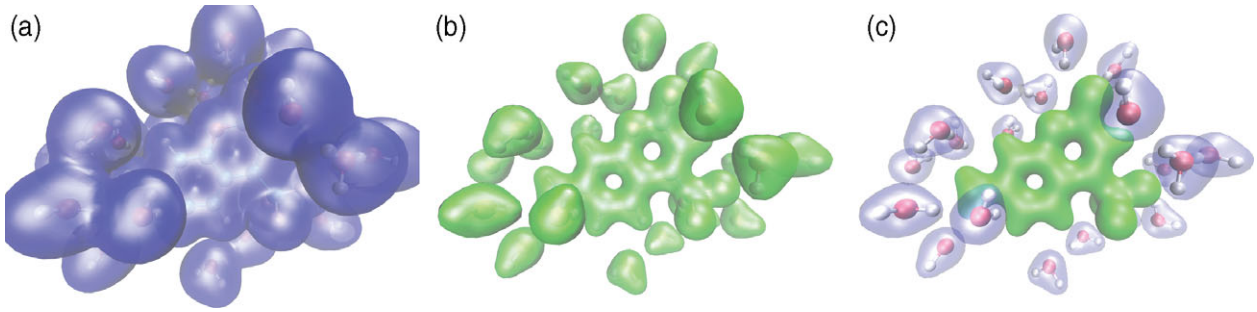

FIGURE 1 | Schematic illustration of the different theoretical approaches available for large molecular systems, using the example of aminocoumarin C151 surrounded by twenty water molecules. (a) In conventional KS-DFT, a single calculation is performed for the full system. (b) In subsystem DFT, the system is split into fragments, and the densities of all fragments are optimized self-consistently. (c) In frozen-density embedding theory, an approximate density is used for the environment, and only the density of the active subsystem is optimized.

a simple isolated molecule calculation on system *B*. This can be improved by an iterative protocol known as "freeze-and-thaw" (see below),[32] but even in this case some negative areas usually remain. In fact, it has been argued that in the case of such nonadmissible frozen densities, the variational problem in FDE is ill-posed.[33,34]

This formal difficulty disappears if we adopt a different point of view—disconnected from a subsystem DFT framework—and instead define the target density of FDE rigorously as the density of the active system that minimizes the total energy of the total system, given an arbitrary frozen environment density.[35,36] If we follow the original strategy[17] and express ρ_A by a Kohn–Sham like system with a set of orbitals $\{\psi_{i_A}\}$, this means that we define our target density as the density resulting from the set of orbitals that minimizes the functional,

$$\begin{aligned} E_{\mathrm{FDE}}[\{\psi_{i_A}\}, \rho_B^{\mathrm{frozen}}] = {} & T_s[\{\psi_{i_A}\}] + T_s[\rho_B^{\mathrm{frozen}}] \\ & + T_s^{\mathrm{nad}}[\rho_A, \rho_B^{\mathrm{frozen}}] \\ & + V_{\mathrm{nuc}}[\rho_A + \rho_B^{\mathrm{frozen}}] \\ & + J[\rho_A + \rho_B^{\mathrm{frozen}}] \\ & + E_{\mathrm{xc}}[\rho_A + \rho_B^{\mathrm{frozen}}]. \end{aligned} \quad (33)$$

As a consequence, FDE is no longer able to lead to the exact ground state energy and density of the total system (not even in principle), but can only yield an upper bound for the energy.[37] It can, therefore, not be considered an alternative to Kohn–Sham DFT, unless the chosen frozen density happens to be admissible in the sense mentioned above. In that case, the target density is again given by Eq. (32).

The restriction to a Kohn–Sham like system *A* can be lifted, and other quantum mechanical descriptors such as reduced density matrices[38] or multideterminantal wave functions[35] can instead be used for subsystem *A*. Hence, the v_s-representability condition can be lifted, and one can argue that FDE defined in this way is more generally applicable than subsystem DFT. As far as the environment is concerned, this holds even when embedding a Kohn–Sham-like system, as is reflected, for example, in applications involving statistically averaged environmental densities.[39]

To overcome the restriction resulting from the first point of view, Gritsenko and Visscher formulated a related embedding approach in which the active subsystem is not represented by its density, but by a "density orbital".[33] This way, the active subsystem can account for regions in which its electron density has to become negative. However, an implementation of this density-orbital embedding method has not been presented so far.

Subsystem DFT and FDE in Practice

Another point of view on the relation of subsystem DFT and FDE is that FDE is an approximation to subsystem DFT, in which not the entire variational freedom of optimizing all subsystem densities is used, but some of the subsystems' densities are kept fixed at a chosen starting approximation. In other words, a constrained minimization of the total energy functional in Eq. (24) is carried out.[40] This directly reflects how the two theories are connected in computational practice: In so-called *freeze-and-thaw* cycles,[32] the roles of active and environmental system in FDE calculations are iteratively interchanged until all subsystem densities are converged. This procedure thus generalizes FDE (in a variational sense) and makes it equivalent to a fully variational subsystem DFT. Interestingly, one could argue that such a freeze-and-thaw strategy should not even be necessary if the correct nonadditive kinetic energy functional was known, provided

the initially chosen frozen density is v_s-representable (see also Ref 34). In practice, however, *freeze-and-thaw* can be helpful to improve the starting density. Physically speaking, it allows for a fully self-consistent polarization of the subsystem densities.

Since it is essentially impossible in such computational applications to draw the line between what might be called "iteratively improved FDE" and "not fully self-consistent subsystem DFT," the term "frozen-density embedding" (FDE) is often used as a more general expression for multilevel simulation methods based on a density partitioning. We will, in subsequent parts of this review, distinguish between the two expressions where possible and unambiguous.

Nonuniqueness of the Density Partitioning

A conceptual problem that arises in subsystem DFT is that there may be infinitely many ways to obtain a correct partitioning.[41] As an example, consider that two subsystem densities,

$$\rho_A(\mathbf{r}) + \rho_B(\mathbf{r}) = \rho_{\text{tot}}(\mathbf{r}), \tag{34}$$

sum up to the correct total density $\rho(\mathbf{r})$. Then also the two densities

$$\tilde{\rho}_A(\mathbf{r}) = \rho_A(\mathbf{r}) + \delta\rho(\mathbf{r}) \tag{35}$$

$$\tilde{\rho}_B(\mathbf{r}) = \rho_B(\mathbf{r}) - \delta\rho(\mathbf{r}) \tag{36}$$

with $\delta\rho(\mathbf{r})$ arbitrary (but integrating to zero to ensure the correct number of electrons per subsystem) will give rise to the correct total density and identical total energies. However, if an approximate functional is used for the nonadditive kinetic energy, these different partitionings are usually not equivalent and correspond to different total energies.

Carter and co-workers have devised a way to avoid the nonuniqueness of the density partitioning by requiring that active system and environment share the same embedding potential, that is, $v_{\text{emb}}^{(A)}(\mathbf{r}) = v_{\text{emb}}^{(B)}(\mathbf{r})$.[41] This idea originates from the partition density-functional theory (PDFT) of Wasserman and co-workers, which is a generalization of subsystem DFT.[42,43] In PDFT, the system of interacting fragments is mapped to an effective system of noninteracting fragments sharing a common embedding potential (called partition potential in the context of PDFT), which is found as the Lagrange multiplier in a functional minimization of the sum-of-fragment energies. PDFT is formulated without constraints on the electron numbers, so that fractional occupation numbers may occur for the fragments. In fact, the total energy is minimized with respect to the particle numbers within all fragments, and only the total number of electrons is fixed. Within PDFT, it can be shown that a common embedding potential for the active subsystem and the environment exists.[44] On the other hand, in the case of integer electron numbers per subsystem the existence of a common embedding potential has to be assumed and only its uniqueness can be established.[41]

THE EMBEDDING POTENTIAL

General Properties of the Embedding Potential

The embedding potential arising in subsystem DFT and FDE, given in Eq. (27), has a number of important properties. In particular in comparison with more approximate, empirical embedding potentials, there are several differences that should be stressed:

- This embedding potential is exact in the limit of exact functionals. Provided that the v_s-representability conditions are met, it will thus lead to the exact total density, that is, subsystem DFT is equivalent to conventional KS-DFT in this limit.
- The main contribution to the embedding potential in the active region, in particular for weakly overlapping densities, are usually the electrostatic potentials of the nuclei and the electrons in the frozen environment. These contributions are always treated exactly in subsystem DFT and FDE. In contrast, most other subsystem methods, such as QM/MM approaches,[45,46] employ additional approximations for these contributions.
- The embedding potential also contains short-range quantum mechanical effects. Among these, the exchange–correlation effects can be treated within the same approximations as used in KS-DFT calculations.
- In addition, also effects usually referred to as Pauli repulsion are included through the kinetic energy contribution.[47] For this part, one can either employ additional approximations, or the kinetic energy contributions can be treated exactly with reconstruction methods. These different options will be explored further in this section.
- In the case of spin-DFT (see, e.g., the recent review in Ref 48), also the embedding potential becomes spin dependent, and the FDE embedding potential can, therefore, describe spin-polarization effects.[41,49–51]

For polar environments, one can argue that a proper representation of the electrostatic terms, including polarization (in the fully self-consistent subsystem DFT variant), is the most important advantage over empirical point-charge or general multipole models for the environmental electrostatic effect. However, a problem well known in pure electrostatic embedding schemes is the electron-leak problem (also called electron spill-out or overpolarization).[4,52] If no additional contributions accounting for Pauli repulsion are present in the embedding potential, electrons of the active subsystem will unphysically localize at the nuclei of the frozen environment, provided the basis set is sufficiently flexible. In a study on electron-density topologies, it was shown that electrostatic-only embedding yields seemingly good results as long as the basis set is restricted to the active subsystem, whereas including basis functions of the frozen subsystem in a so-called supermolecular basis set expansion leads to a drastic failure.[31] More recently, Fradelos and Wesołowski have investigated numerical instabilities and overpolarization effects arising when neglecting the intermolecular Pauli repulsion.[47,53]

Therefore, the use of the full electrostatic embedding potential makes it necessary to also include short-range quantum-mechanical contributions. In the FDE embedding potential, these are accounted for by the exchange–correlation and kinetic energy contributions. However, the commonly used approximations for the nonadditive kinetic energy (see below) might not always be accurate enough to prevent the electron-leak problem completely.[54–56] For an overview, see Ref 23.

The Nonadditive Kinetic Energy

While the electrostatic contributions to the embedding potential in FDE and subsystem DFT can be treated exactly and for the exchange–correlation component the same approximations as employed in conventional KS-DFT can be used, the kinetic energy part requires more attention. This contribution arises from the nonadditive kinetic energy [Eqs. (22) and (23)]. It cannot be calculated directly, because the KS orbitals $\{\psi_i\}$ of the full system are not available in subsystem DFT.

The situation may be considered different for subsystems with densities constructed from subsets of the orthogonal orbitals of a (spin compensated) Kohn–Sham solution. For the special case of two subsystems (A and B), such pairs of densities have been called v^{AB}-representable pairs of densities,[22,57] and this can easily be generalized to $v^{ABC\ldots}$-representable sets of densities obtained in a similar manner for many subsystems. In the two-partitioning case, consider the ground state density $\rho^{(0)}$ of the supersystem and the corresponding ground state Kohn–Sham orbitals $\{\psi_i^{(0)}\}$. Then, we assign a subset of these orbitals to one of the subsystems, and the remaining orbitals to the other,

$$\begin{aligned} T_s[\rho^{(0)}] = T_s\left[\left\{\psi_i^{(0)}\right\}\right] &= \sum_{i=1}^{n}\left\langle\psi_i^{(0)}\left|-\nabla^2/2\right|\psi_i^{(0)}\right\rangle \\ &= \sum_{j=1}^{n_A}\left\langle\psi_j^{(0)}\left|-\nabla^2/2\right|\psi_j^{(0)}\right\rangle \\ &\quad + \sum_{k=n_A+1}^{n_A+n_B}\left\langle\psi_k^{(0)}\left|-\nabla^2/2\right|\psi_k^{(0)}\right\rangle \end{aligned} \tag{37}$$

where n_A and n_B are the numbers of electrons in systems A and B, respectively, with $n = n_A + n_B$, and

$$\rho_A(\mathbf{r}) = \sum_{j=1}^{n_A}\left|\psi_j^{(0)}(\mathbf{r})\right|^2 \quad \text{and} \quad \rho_B(\mathbf{r}) = \sum_{k=n_A+1}^{n_A+n_B}\left|\psi_k^{(0)}(\mathbf{r})\right|^2. \tag{38}$$

The orbitals are thus assumed to be ordered in a proper way, reflecting the definition of the subsystems. If we express the kinetic energy through a given set of orbitals, we can write (see, e.g., Ref 58),

$$T_s\left[\left\{\psi_i^{(0)}\right\}\right] = T_s\left[\left\{\psi_i^{(0)}\right\}_{i\in A}\right] + T_s\left[\left\{\psi_i^{(0)}\right\}_{i\in B}\right], \tag{39}$$

from which one could conclude that the nonadditive kinetic energy as a functional of the two sets of orthogonal orbitals vanishes for v^{AB}-representable pairs of densities,

$$T_s^{\mathrm{nad}}\left[\left\{\psi_i^{(0)}\right\}_{i\in A}, \left\{\psi_i^{(0)}\right\}_{i\in B}\right] = 0. \tag{40}$$

However, the Levy-constrained search definition of the kinetic energy density functional $T_s[\rho]$ [cf. Eq. (10)] requires that the orbitals are those of the ground state, which is in general not the case for orbitals as chosen here. Thus, we have

$$T_s[\rho_{A/B}] \geq T_s\left[\left\{\psi_i^{(0)}\right\}_{i\in A/B}\right] \tag{41}$$

and it can only be shown in general that the nonadditive kinetic energy as a functional of the densities is nonnegative,[57]

$$T_s^{\mathrm{nad}}[\rho_A, \rho_B] \geq 0. \tag{42}$$

At this point, it is important to note that none of the above implies that the corresponding nonadditive

kinetic potential vanishes. For explicit examples, see Ref 59. As shown in Ref 58, a practical strategy can be to employ v^{AB}-representable pairs of densities and the corresponding sets of orthogonal orbitals and to introduce a projection operator that keeps the orbitals of one subsystem orthogonal to those of the other one.

Finally, it is interesting to note that the nonadditive kinetic energy vanishes for subsystem densities that do not overlap, that is, if $\rho_A(\mathbf{r})\rho_B(\mathbf{r}) = 0$ at every point in space (see Appendix A in Ref 60).

Decomposable Approximations for the Nonadditive Kinetic Potential

The most straightforward strategy for approximating the nonadditive kinetic energy and the nonadditive kinetic potential is the use of an approximate, explicitly density-dependent kinetic energy functional $\tilde{T}_s[\rho]$. In such so-called decomposable approximations, one uses

$$\tilde{T}_s^{\mathrm{nad}}[\{\rho_I\}] = \tilde{T}_s[\rho_{\mathrm{tot}}] - \sum_I \tilde{T}_s[\rho_I] \tag{43}$$

for the nonadditive kinetic energy and

$$\tilde{v}_{\mathrm{kin}}^{\mathrm{nad}}[\rho_K, \rho_{\mathrm{tot}}](\mathbf{r}) = \frac{\delta \tilde{T}_s^{\mathrm{nad}}[\{\rho_I\}]}{\delta\rho_K(\mathbf{r})} = \frac{\delta \tilde{T}_s[\rho_{\mathrm{tot}}]}{\delta\rho_{\mathrm{tot}}(\mathbf{r})} - \frac{\delta \tilde{T}_s[\rho_K]}{\delta\rho_K(\mathbf{r})}, \tag{44}$$

for the nonadditive kinetic potential. Here and in the following, the tilde is used to indicate approximate functionals. Thus, the problem of approximating the nonadditive kinetic energy reduces to the one of finding suitable approximate kinetic energy functionals. Note, however, that in subsystem DFT such approximate kinetic energy functionals are only used for the *nonadditive* part of the kinetic energy, which is in many cases only a small part of the total kinetic energy. Therefore, finding suitable approximations for subsystem DFT is simpler than finding explicitly density-dependent kinetic energy functionals that can approximate the full kinetic energy accurately to allow for orbital-free DFT calculations.[61]

There are certain model systems for which the kinetic energy functional can be specified exactly. One example is the uniform electron gas, for which the noninteracting kinetic energy is given by the Thomas–Fermi (TF) expression,[18,19]

$$T_s^{\mathrm{TF}}(\rho) = C_F\rho^{5/3}, \quad \text{with} \quad C_F = \frac{3}{10}(3\pi^2)^{2/3}. \tag{45}$$

When applied to a nonuniform electron density, this turns into the local-density approximation (LDA) for the kinetic energy,

$$\tilde{T}_s^{\mathrm{TF}}[\rho] = \tilde{T}_s^{\mathrm{LDA}}[\rho] = C_F \int \rho^{5/3}(\mathbf{r})\mathrm{d}\mathbf{r}. \tag{46}$$

On the basis of this expression, we can obtain an LDA approximation for the nonadditive kinetic energy,

$$\begin{aligned}\tilde{T}_s^{\mathrm{nad,LDA}}[\{\rho_I\}] &= \tilde{T}_s^{\mathrm{TF}}[\rho] - \sum_I \tilde{T}_s^{\mathrm{TF}}[\rho_I] \\ &= C_F \int \left[\rho^{5/3}(\mathbf{r}) - \sum_I \rho_I^{5/3}(\mathbf{r})\right]\mathrm{d}\mathbf{r}\end{aligned} \tag{47}$$

The corresponding nonadditive kinetic potential for subsystem K is given as

$$\tilde{v}_{\mathrm{kin}}^{\mathrm{nad,LDA}}[\rho_K, \rho](\mathbf{r}) = \frac{5}{3}C_F\left\{\rho^{2/3}(\mathbf{r}) - \rho_K^{2/3}(\mathbf{r})\right\}. \tag{48}$$

Another class of exactly known cases are one-electron and spin-compensated two-electron systems (i.e., systems in which there is only one Kohn–Sham orbital). Here, the kinetic energy is given exactly by the von Weizsäcker expression,

$$\tilde{T}_s^{\mathrm{vW}}[\rho] = \frac{1}{8}\int \frac{|\nabla\rho(\mathbf{r})|^2}{\rho(\mathbf{r})}\mathrm{d}\mathbf{r}. \tag{49}$$

This implies that a corresponding nonadditive kinetic-energy functional will be exact if the von Weizsäcker functional is exact both for the total system and all the subsystems.

The kinetic energy potential arising from the von Weizsäcker functional has the form,[18]

$$\tilde{v}_{\mathrm{kin,vW}}(\mathbf{r}) = \frac{\delta \tilde{T}_s^{\mathrm{vW}}[\rho]}{\delta\rho(\mathbf{r})} = -\frac{1}{4}\frac{\nabla^2\rho(\mathbf{r})}{\rho(\mathbf{r})} + \frac{1}{8}\frac{|\nabla\rho(\mathbf{r})|^2}{\rho(\mathbf{r})^2}. \tag{50}$$

Note that the negative of the von Weizsäcker potential also arises (up to a constant shift) if one inverts the Schrödinger equation for a single orbital with $|\psi(\mathbf{r})|^2 = \rho(\mathbf{r})$.

These two kinetic energy functionals, $\tilde{T}_s^{\mathrm{TF}}$ and $\tilde{T}_s^{\mathrm{vW}}$, can be used to construct the lowest order approximations to the true $T_s^{\mathrm{nad}}[\{\rho_I\}]$ in a regular density-gradient expansion (DGE; also known as gradient expansion approximation, GEA, or conventional gradient expansion, CGE),[18,22,61,62]

$$\tilde{T}_s^{\mathrm{nad,DGE0}}[\{\rho_I\}] = \tilde{T}_s^{\mathrm{nad,TF}}[\{\rho_I\}], \tag{51}$$

$$\tilde{T}_s^{\mathrm{nad,DGE2}}[\{\rho_I\}] = \tilde{T}_s^{\mathrm{nad,TF}}[\{\rho_I\}] + \frac{1}{9}\tilde{T}_s^{\mathrm{nad,vW}}[\{\rho_I\}], \tag{52}$$

$$\tilde{T}_s^{\mathrm{nad,DGE4}}[\{\rho_I\}] = \tilde{T}_s^{\mathrm{nad,TF}}[\{\rho_I\}] + \frac{1}{9}\tilde{T}_s^{\mathrm{nad,vW}}[\{\rho_I\}] + \tilde{T}_s^{\mathrm{nad,H}}[\{\rho_I\}]. \quad (53)$$

$\tilde{T}_s^{\mathrm{nad,H}}$ is constructed in the usual way from the underlying kinetic energy functional,[63]

$$\tilde{T}_s^{H}[\rho] = \frac{(3\pi^2)^{-2/3}}{540}\int \rho^{1/3}\left[\left(\frac{\nabla^2\rho}{\rho}\right)^2 - \frac{9}{8}\left(\frac{\nabla^2\rho}{\rho}\right)\left(\frac{\nabla\rho}{\rho}\right)^2 + \frac{1}{3}\left(\frac{\nabla\rho}{\rho}\right)^4\right]\mathrm{d}\mathbf{r}. \quad (54)$$

Note that only even terms appear in the regular gradient expansion for the kinetic energy. Full details on the density-gradient expansion can be found in chapter 5 of Ref 62.

If used self-consistently, the DGE route is neither very successful for the kinetic energy in general[18] nor for the nonadditive kinetic energy in particular.[22] There has therefore been a large activity in the field of generalized gradient approximation (GGA) functionals for the kinetic energy, which can be expressed as

$$\tilde{T}_s^{\mathrm{GGA}}[\rho] = C_{\mathrm{TF}}\int \rho^{5/3}(\mathbf{r})F\big(s(\mathbf{r})\big)\mathrm{d}\mathbf{r}, \quad (55)$$

where the quantity $F(s)$ is known as the *enhancement factor*. It is usually expressed in terms of one of the dimensionless quantities

$$x(\mathbf{r}) = \frac{|\nabla\rho(\mathbf{r})|}{\rho^{4/3}(\mathbf{r})}, \quad (56)$$

or

$$s(\mathbf{r}) = \frac{x(\mathbf{r})}{2(3\pi^2)^{1/3}}. \quad (57)$$

The latter is called *reduced density gradient*. Nonadditive kinetic energy functionals can be constructed from such GGA-type functionals in the usual (decomposable) way.

Several GGA-type kinetic energy functionals have been constructed using the conjointness hypothesis.[64,65] Lee et al. assumed that the same form of the enhancement factor can be used for exchange and kinetic energy functionals[64] and constructed a kinetic energy functional based on Becke's 1988 exchange functional known as B88.[66] A widely used functional constructed from this recipe is derived from the Perdew–Wang (PW91) exchange functional[67] and is thus often denoted as PW91k. Since the parameters in this functional were adapted for the kinetic energy by Lembarki and Chermette,[68] it is also known as the LC94 functional. Table 1 collects a number of enhancement factors used for GGA-type kinetic-energy functionals (a more extensive overview is given in Ref 69).

Another class of kinetic energy functionals builds in the known linear response of a homogeneous, noninteracting electron gas, which is given by the Lindhard response function.[61,81,82] Other recent developments in this field are given in Ref 83. Since the resulting functionals are nonlocal in space, their evaluation is much more demanding than that of (semi)local functionals.[78,84] They can be computed rather efficiently in reciprocal space for periodic systems, but care has to be taken for nonperiodic systems, for which Choly and Kaxiras suggested an alternative way of computation.[82] For more recent progress in the field of nonlocal kinetic energy functionals, see the work by Carter and co-workers.[85,86]

For spin-polarized cases, we can use the spin-scaling relation[87] to express T_s as a functional of the α- and β-spin density components $\rho_{\alpha/\beta}$,

$$T_s[\rho_\alpha,\rho_\beta] = \frac{1}{2}T_s[2\rho_\alpha] + \frac{1}{2}T_s[2\rho_\beta]. \quad (58)$$

Conversely, we can also express the functional for the spin-compensated system as

$$T_s[\rho] = 2T_s[(\rho/2),0]. \quad (59)$$

As noted for the corresponding case of exchange functionals by Scuseria and Staroverov,[88] we mention that kinetic energy functionals are often expressed in the spin-compensated form $T_s[\rho]$ only, whereas the spin-polarized form $T_s[\rho_\alpha,\rho_\beta]$ is usually the one that is actually used. The two can be interconverted using the relationships given above. Differences in prefactors in the functionals can arise depending on which form is used. For the Thomas–Fermi functional in its spin-polarized form, we get

$$\tilde{T}_s^{\mathrm{TF}}[\rho_\alpha,\rho_\beta] = 2^{2/3}C_F\int\left(\rho_\alpha^{5/3}(\mathbf{r}) + \rho_\beta^{5/3}(\mathbf{r})\right)\mathrm{d}\mathbf{r} \quad (60)$$

$$= 2^{2/3}\left(\tilde{T}_s^{\mathrm{TF}}[\rho_\alpha] + \tilde{T}_s^{\mathrm{TF}}[\rho_\beta]\right), \quad (61)$$

whereas the von Weizsäcker functional in the spin-polarized case is given as

$$\tilde{T}_s^{\mathrm{vW}}[\rho_\alpha,\rho_\beta] = \frac{1}{8}\int\frac{|\nabla\rho_\alpha(\mathbf{r})|^2}{\rho_\alpha(\mathbf{r})}\mathrm{d}\mathbf{r} + \frac{1}{8}\int\frac{|\nabla\rho_\beta(\mathbf{r})|^2}{\rho_\beta(\mathbf{r})}\mathrm{d}\mathbf{r} \quad (62)$$

$$= \tilde{T}_s^{\mathrm{vW}}[\rho_\alpha] + \tilde{T}_s^{\mathrm{vW}}[\rho_\beta]. \quad (63)$$

If we want to rewrite a particular spin-compensated GGA functional as a spin-polarized one, we again use

TABLE 1 | Enhancement Factors $F(s)$ of Typical Kinetic Energy Functionals. The Constant β is Defined as $\beta = 2(6\pi^2)^{1/3}$, respectively. The Parameters in the LC94 (or PW91k) Functional Are $A = 76.320$, $A_1 = 0.093907$, $A_2 = 0.26608$, $A_3 = 0.0809615$, $A_4 = 100.00$, $B_1 = 0.57767 \cdot 10^{-4}$. The s-Dependent Parameter in APBEKint and revAPBEKint is $\mu_s^{\text{int}}(s) = (\frac{5}{9} + 5 \cdot 0.23899 s^2)/(3 + 5s^2)$.

Name	Acronym	$F(s)$	Reference
Thomas–Fermi	TF	1	70,71
von Weizsäcker	vW	$\frac{5}{3}s^2$	72
2nd order DGE	DGE2	$1 + \frac{5}{27}s^2$	63
modified DGE2	MGEA2	$1 + \frac{5}{27} \cdot 1.290 s^2$	73
Ou-Yang, Levy	OL1	$1 + \frac{5}{27}s^2 + 0.0187\beta s$	74
	OL2	$1 + \frac{5}{27}s^2 + \frac{0.0245 \cdot \beta s}{1 + 2^{5/3}\beta s}$	74
Lee, Lee, Parr	LLP	$1 + \frac{0.0044188\,(\beta s)^2}{1 + 0.0253\,\beta s \sinh^{-1}(\beta s)}$	64
conjoint Perdew, Wang	PW86	$(1 + 1.296 s^2 + 14 s^4 + 0.2 s^6)^{1/15}$	75
Tran, Wesołowski	TW	$1 + \frac{0.2319 s^2}{1 + \frac{0.2319}{0.8438}s^2}$	76
Thakkar	TK92	$1 + \frac{0.0055(\beta s)^2}{1 + 0.0253\,\beta s \sinh^{-1}(\beta s)} - \frac{0.072\beta s}{1 + 2^{5/3}\beta s}$	77
Lembarki, Chermette	PW91k or LC94	$\frac{1 + A_1 s \sinh^{-1}(As) + (A_2 - A_3 e^{-A_4 s^2})s^2}{1 + A_1 s \sinh^{-1}(As) + B_1 s^4}$	68
Karasiev, Trickey, Harris	PBE2	$1 + \frac{2.0309 s^2}{1 + 0.2942 s^2}$	78
	PBE3	$1 - \frac{3.7425 s^2}{1 + 4.1355 s^2} + \frac{50.258 s^4}{(1 + 4.1355 s^2)^2}$	78
	PBE4	$1 - \frac{7.2333 s^2}{1 + 1.7107 s^2} + \frac{61.645 s^4}{(1 + 1.7107 s^2)^2} - \frac{93.683 s^6}{(1 + 1.7107 s^2)^3}$	78
	exp4	$0.8524(1 - e^{-199.81 s^2}) + 1.2264(1 - e^{-4.3476 s^4})$	78
asymptotic PBE	APBEK	$1 + \frac{0.23889 s^2}{1 + \frac{0.23889}{0.804}s^2}$	79
revised APBEK	revAPBEK	$1 + \frac{0.23889 s^2}{1 + \frac{0.23889}{1.245}s^2}$	79
modified APBEK	APBEKint	$1 + \frac{\mu_s^{\text{int}}(s) s^2}{1 + \frac{\mu_s^{\text{int}}(s)}{0.804}s^2}$	80
modified revAPBEK	revAPBEKint	$1 + \frac{\mu_s^{\text{int}}(s) s^2}{1 + \frac{\mu_s^{\text{int}}(s)}{1.245}s^2}$	80

the spin-scaling relation,

$$\tilde{T}_s^{\mathrm{GGA}}[\rho_\alpha, \rho_\beta] = \frac{1}{2}\sum_\sigma C_{\mathrm{TF}} \int (2\rho_\sigma)^{5/3} F(s_\sigma)\mathrm{d}\mathbf{r}, \quad (64)$$

$$= 2^{2/3} C_{\mathrm{TF}} \int \sum_\sigma \rho_\sigma^{5/3} F(s_\sigma)\mathrm{d}\mathbf{r}, \quad (65)$$

where $\sigma \in \{\alpha, \beta\}$, and s_σ is given as

$$s_\sigma = \frac{|\nabla(2\rho_\sigma)|}{2(2\rho_\sigma)^{4/3}(3\pi^2)^{1/3}} = \frac{|\nabla\rho_\sigma|}{2\rho_\sigma^{4/3}(6\pi^2)^{1/3}} = \frac{x_\sigma}{2(6\pi^2)^{1/3}}. \quad (66)$$

The last equality defines $x_\sigma = |\nabla\rho_\sigma|/\rho_\sigma^{4/3}$. We can thus easily express any GGA-type functional known in the spin-compensated form as a spin-polarized one by (i) using s_σ instead of s as an argument for the enhancement factor, (ii) summing over spin components σ, and (iii) including a prefactor of $2^{2/3}$. Note that using x and x_σ instead of s and s_σ as a variable for the enhancement factor makes it necessary to account for these prefactors by converting the additional coefficients entering the enhancement factor.

Calculation of Charge Densities and Multipole Moments

The accuracy of the approximate embedding potentials used in subsystem DFT governs the quality of the subsystem electron densities. Hence, the sum of the subsystem densities is the key benchmark quantity to test the suitability of a particular approximate potential. Since both subsystem and KS-DFT have to make an approximation for the exchange–correlation energy functional $\tilde{E}_{\mathrm{xc}}[\rho]$ and its functional derivatives, and since this approximation can be chosen consistently if pure density functionals are employed, subsystem DFT should be able to reproduce the electron density distribution of a KS-DFT calculation employing the same expression for $\tilde{E}_{\mathrm{xc}}[\rho]$. This provides a protocol for assessing the error introduced by the approximations employed for the nonadditive kinetic potential by comparing the electron density from a fully self-consistent subsystem DFT calculation (i.e., a calculation in which the densities of all subsystems are updated in freeze-and-thaw iterations) to the one from a supermolecular KS-DFT calculation.

However, the supermolecular results can only be reproduced exactly if the basis set is chosen appropriately. For direct comparability with Kohn–Sham DFT, a so-called supermolecular expansion should be used, that is, a basis set covering all atoms of the total system in all of the subsystem calculations.[89,90] However, for practical applications one would prefer a monomer (subsystem) basis set,[91] which is also the natural choice to have full benefit of the computational advantages of a subsystem approach. Often, such a monomer expansion already provides enough flexibility, in particular if large basis sets are used. Obvious exceptions are systems with strong polarization or charge-transfer character at the boundary between subsystems. A strategy that can keep the computational cost manageable even for large total systems is to employ a monomer expansion plus a few additional ghost basis functions in the boundary region where the polarization shall be described. Besides the generally (much) smaller computational cost per subsystem calculation, it should also be stressed that subsystem DFT calculations with monomer basis sets are inherently free of basis set superposition errors.

A number of studies of electron densities obtained from subsystem DFT have been performed to assess approximations for the nonadditive kinetic potential.[89,92,93] Note, however, that the accuracy of the electron density does not necessarily correlate with the one of the parent energy functional $\tilde{T}_s^{\mathrm{nad}}[\{\rho_I\}]$.[89] We will return to the calculation of the interaction energies from subsystem DFT in the section Interaction Energy Calculations. Nevertheless, the accuracy of the resulting electron densities and of energetic properties have often been considered together when recommending approximate functionals for the use in subsystem DFT and FDE.[89,92,94] Therefore, in the following we will highlight some recent systematic studies that only focused on the electron density or on quantities derived from it.

A topological electron density analysis has been performed for several hydrogen-bonded systems by Kiewisch et al.,[31] comparing the densities from fully self-consistent subsystem DFT calculations with the TF and PW91k nonadditive kinetic energy functions to reference densities from supermolecular KS-DFT calculations. This study included systems connected through several hydrogen bonds and the strong symmetric hydrogen bond in $F{-}H{-}F^-$. It was shown that even in those cases the qualitative changes in the electron density topology, for example, the coordinates of bond critical points, can be reproduced by FDE. However, usually it was necessary to employ a supermolecular basis for good agreement. More strongly interacting systems such as coordination compounds were investigated in Ref 95, where it was found that systems like ammonia borane can still be reasonably handled by subsystem DFT, whereas it fails dramatically for transition-metal complexes with π-backbonding like $Cr(CO)_6$. Another study on weak covalent bonds with subsystem DFT was presented in Ref 96, where noble gas–gold fluoride complexes were studied.[96] The authors came to the

conclusion that none of the standard approximations (i.e., LDA or GGA kinetic energy functionals) worked for these systems, even though the interactions are only weak. Hence, it is more the type of interaction that determines whether subsystem DFT with standard approximations is applicable: For systems with covalent interactions, this is typically not the case.

Dipole and higher multipole moments can be used as simple descriptors for the electron-density distribution and have therefore been used as a quality measure for FDE and subsystem DFT calculations from early on. The dipole moment of water in water, for instance, was studied already in 1994 with limited success,[97] probably because of a too small basis. A later study[98] reported a much larger increase in the dipole moment (from 1.80 to 2.71 D) for an aqueous environment and also showed that higher multipole moments were in good agreement with those from polarizable classical force field methods. Other early studies presented dipole moments for hydrogen-bonded dimers and found them in good agreement with supermolecular reference results.[89] Beyhan et al. calculated dipole moments in their study on covalently bonded noble gas–gold fluoride complexes. Interestingly, the PBE2 kinetic energy functional[78] employed for $\tilde{T}_s^{\mathrm{nad}}$ with a supermolecular basis showed very good results for all noble gases tested, whereas essentially all other functionals failed. Again, this case has to be interpreted with caution, as the system comprises a weak covalent bond. Laricchia et al. have compared subsystem DFT densities and dipole moments for calculations within the generalized Kohn–Sham context, which employed hybrid exchange–correlation functionals for the intrasubsystem contributions, whereas the intersubsystem contributions were approximated by GGA-type functionals.[28] They reported an increased accuracy for those calculations employing hybrid functionals.

We would like to take the opportunity to illustrate the features of subsystem DFT with a small example calculation. Employing the Becke88 exchange functional[66] and the Perdew1986 correlation functional (together in the following denoted as BP86) as implemented in the Amsterdam Density Functional (ADF) program,[99–101] the triple-zeta plus polarization (TZP) basis set from the ADF basis set library, and the reparameterized PW91k (LC94) functional for a decomposable approximation to T_s^{nad} in the case of subsystem DFT calculations, we calculated the dipole moment for several oligomers of HCN both with subsystem and with Kohn–Sham DFT. For this comparison, we employed the optimized (BP86/TZP) monomer structure, which was copied along the molecular axis in such a way that

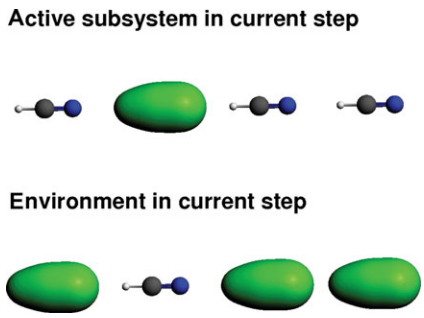

FIGURE 2 | Structure of the HCN_n systems investigated here (example with $n = 4$) and schematic representation of a certain step in the subsystem DFT calculation, in which the density of the second monomer is determined under the influence of an embedding potential derived from the density of the other systems (densities represented through isosurface plots).

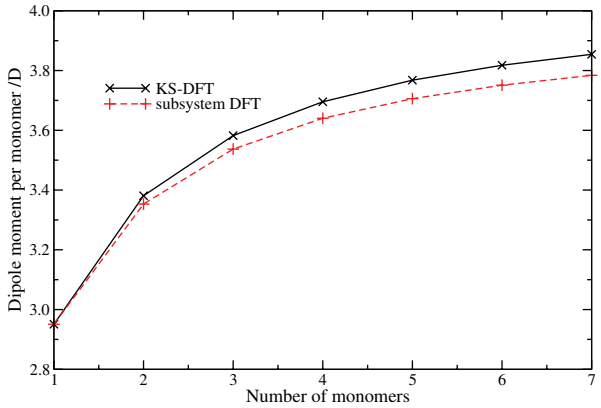

FIGURE 3 | Average dipole moment of the HCN_n systems ($n = 1 \ldots 7$) from subsystem DFT (BP86/TZP/PW91k) and KS-DFT (BP86/TZP).

the carbon–carbon distance between two neighboring HCN molecules was as large as the corresponding distance in the BP86/TZP-optimized dimer (4.43 Å; see Figure 2). The H-bonding distance was thus 2.19 Å. The results for the average dipole moment per monomer are shown in Figure 3, where it can clearly be seen that there is a cooperative effect in the dipole moment: The more monomers are added, the larger is the average dipole moment. Subsystem DFT and KS-DFT values are in nice agreement, although the former leads to slightly smaller changes: The increase from $(HCN)_1$ to $(HCN)_7$ is 0.90 D for KS-DFT and 0.83 D for subsystem DFT. However, it should be noted that subsystem DFT was applied here with a monomer expansion (and three freeze-and-thaw cycles), so that the dipole moments are not affected by the basis set superposition error. A nice feature of subsystem DFT is that a very easy analysis of the results is facilitated. In contrast to the supermolecular

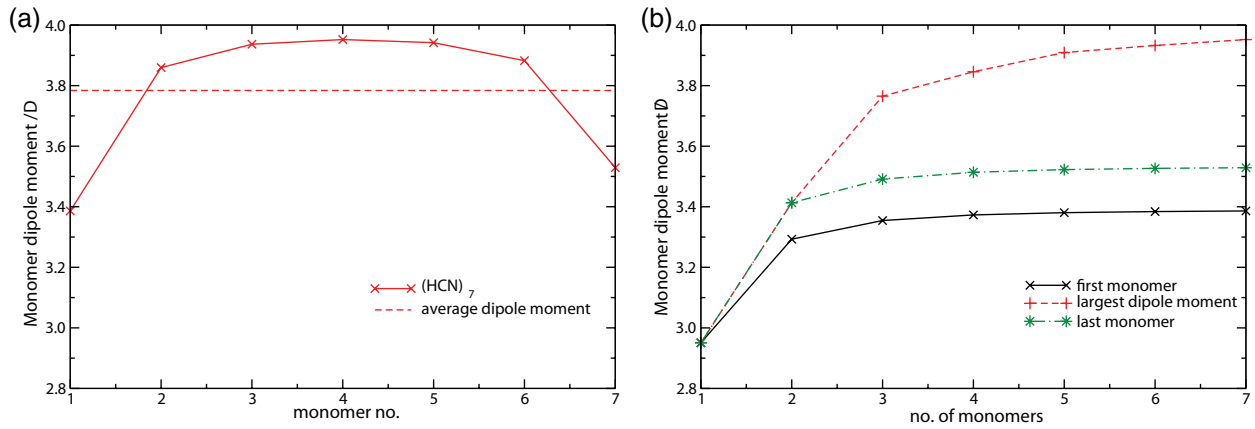

FIGURE 4 | Analysis of the dipole moment of the HCN_n chains from subsystem DFT (BP86/TZP/PW91k) calculations; (a) contributions of individual monomers in HCN_7; (b) contributions of first and last monomer in HCN_n chains ($n = 1 \ldots 7$) as well as largest monomer contribution.

KS results, which have to be assigned/partitioned into monomer contributions afterward, the subsystem calculation constructs the total dipole moment from contributions of each of the monomers in the chain, which arise naturally as intermediate quantities in the calculation. For example, Figure 4(a) shows the individual monomer dipole moments from the subsystem DFT calculation on $(HCN)_7$, and Figure 4(b) shows the contributions of the first and last monomer as well as the largest individual dipole moment in the chain as a function of the chain length. Subsystem DFT thus offers great advantages in terms of an analysis of molecular interactions and cooperative effects due to many interacting subunits.

Nondecomposable Approximations for the Nonadditive Kinetic Potential

Instead of using decomposable approximations derived from a parent kinetic energy functional, one can also attempt to approximate the nonadditive kinetic energy or the nonadditive kinetic potential directly. Such approximations are referred to as *nondecomposable approximations*. For those classes of applications in which the desired quantity can be obtained directly from the potential (e.g., the electron density, multipole moments, excitation energies, or several other molecular properties), it can be considered advantageous to construct approximations for this quantity itself, instead of approximating the kinetic energy functional.[94,102,103] This strategy, which is also known in the context of exchange–correlation functionals in Kohn–Sham DFT (see, for example, Refs 104–106), does, however, not allow one to obtain the *energy* of the system from a consistent functional.

For approximating the nonaddive kinetic potential, one promising strategy is to study the exact nonadditive kinetic potential in cases where it is known. This can serve as guidance for developing approximations that can describe covalent bonds between subsystems. The nonadditive kinetic potential is given by

$$v_{\mathrm{kin}}^{\mathrm{nad}}[\rho_K, \rho_{\mathrm{tot}}](\mathbf{r}) = \left.\frac{\delta T_s[\rho]}{\delta\rho(\mathbf{r})}\right|_{\rho(\mathbf{r})=\rho_{\mathrm{tot}}(\mathbf{r})} - \left.\frac{\delta T_s[\rho]}{\delta\rho(\mathbf{r})}\right|_{\rho(\mathbf{r})=\rho_K(\mathbf{r})} = v_{\mathrm{kin}}[\rho_{\mathrm{tot}}](\mathbf{r}) - v_{\mathrm{kin}}[\rho_K](\mathbf{r}). \quad (67)$$

The calculation of this term thus requires the knowledge of the functional derivative of the noninteracting kinetic energy $\delta T_s[\rho]/\delta\rho(\mathbf{r})$ for two different densities, the total electron density $\rho_{\mathrm{tot}}(\mathbf{r})$, and the density of the active subsystem $\rho_K(\mathbf{r})$.

For a given v_s-representable density $\rho(\mathbf{r})$, there exists a potential $v_s[\rho](\mathbf{r})$ that yields this density as the ground state solution of the noninteracting Schrödinger equation, $\left[-\nabla^2/2 + v_s(\mathbf{r})\right]\psi_i(\mathbf{r}) = \epsilon_i\psi_i(\mathbf{r})$. For this potential $v_s[\rho](\mathbf{r})$, the density $\rho(\mathbf{r})$ minimizes the noninteracting energy functional,

$$E_s[\tilde{\rho}] = T_s[\tilde{\rho}] + \int \tilde{\rho}(\mathbf{r}) v_s[\rho](\mathbf{r})\mathrm{d}\mathbf{r} \quad (68)$$

under the constraint that the density integrates to the correct number of electrons. Thus, for this density the corresponding Euler–Lagrange equation

$$\left.\frac{\delta E_s[\tilde{\rho}]}{\delta\tilde{\rho}(\mathbf{r})}\right|_{\tilde{\rho}(\mathbf{r})=\rho(\mathbf{r})} = \left.\frac{\delta T_s[\tilde{\rho}]}{\delta\tilde{\rho}(\mathbf{r})}\right|_{\tilde{\rho}(\mathbf{r})=\rho(\mathbf{r})} + v_s[\rho](\mathbf{r}) = \mu \quad (69)$$

is fulfilled. This provides the possibility to calculate the functional derivative of the noninteracting kinetic

energy as[107]

$$\left.\frac{\delta T_s[\tilde{\rho}]}{\delta\tilde{\rho}(\mathbf{r})}\right|_{\tilde{\rho}(\mathbf{r})=\rho(\mathbf{r})} = -v_s[\rho](\mathbf{r}) + \mu. \tag{70}$$

Thus, except for a constant shift μ, the functional derivative of the noninteracting kinetic energy $\delta T_s[\tilde{\rho}]/\delta\tilde{\rho}$, evaluated for the density $\rho(\mathbf{r})$, is given by the negative of the potential $v_s[\rho]$ that yields this density $\rho(\mathbf{r})$ as its noninteracting ground state. Here, it is important to note that in general the potential $v_s[\rho]$ is different from the effective potential $v_{\text{eff}}[\rho]$. The former is defined by yielding a given ground state density, whereas the latter is calculated from Eq. (15), that is, it is the sum of the nuclear potential for a specific molecular system and of the Coulomb and exchange–correlation potentials evaluating for the given density. The two potentials are equal if and only if ρ is the exact ground state density for the considered molecule.

Applying this result to the kinetic energy component of the embedding potential, we arrive at[102]

$$v_{\text{kin}}^{\text{nad}}[\rho_K, \rho_{\text{tot}}](\mathbf{r}) = v_s[\rho_K](\mathbf{r}) - v_s[\rho_{\text{tot}}](\mathbf{r}) + \Delta\mu, \tag{71}$$

where the constant shift is given by $\Delta\mu = \mu_{\text{tot}} - \mu_K$. Therefore, calculating the kinetic energy part of the embedding potential exactly is possible if we can determine the potentials $v_s[\rho_{\text{tot}}]$ and $v_s[\rho_K]$ that have the total density ρ_{tot} and the density of the active subsystem ρ_K, respectively, as their noninteracting ground states.

Equation (71) can be used to study exact properties of the nonadditive kinetic potential. In Ref 102, the limit of two subsystems at large separation has been investigated. It can be shown that in this limit, the embedding potential at the frozen subsystem should vanish, that is, the kinetic energy contribution has to cancel all other parts of the embedding potential. However, with LDA and GGA approximations the nonadditive kinetic potential is not repulsive enough to achieve such a cancellation. Based on this analysis, a long-distance correction to the nonadditive kinetic potential has been developed, which enforces the correct behavior at the frozen subsystem.[102] Including such a correction results in a nondecomposable approximation to the nonadditive kinetic potential. In a similar spirit, one can enforce the correct form of the nonadditive kinetic potential close to the nuclei of the frozen subsystem (where the electron density is dominated by a single orbital) by switching on a von Weizsäcker term in these regions.[94] The resulting nondecomposable approximation to the nonadditive kinetic energy potential, termed nondecomposable approximant using first and second derivatives (NDSD), has been shown to yield improved electron densities compared to the conventional PW91k approximation. While in computational practice, the two approaches of Refs 94, 102 are similar as far as the *potentials* are concerned, the approach of Ref 94 is more general as it also provides a consistent NDSD *energy* expression (see also the discussion in Refs 108, 109 on whether or not NDSD should formally be considered preferable for the corresponding potential).

If the active subsystem contains only two electrons of opposite spin (i.e., is described by a single KS orbital), the kinetic energy component of the embedding potential can be evaluated (partly) analytically. In this case, the von Weizsäcker functional provides the exact kinetic energy and its functional derivative exactly gives the negative of the potential $v_s[\rho_K^{(2e)}]$ yielding the two-electron density $\rho_K^{(2e)}$, plus a constant shift. Therefore, one has[110]

$$v_{\text{kin}}^{\text{nad}}\left[\rho_K^{(2e)}, \rho_{\text{tot}}\right](\mathbf{r}) = \frac{1}{4}\frac{\nabla^2\rho_K^{(2e)}(\mathbf{r})}{\rho_K^{(2e)}(\mathbf{r})} - \frac{1}{8}\frac{\left|\nabla\rho_K^{(2e)}(\mathbf{r})\right|^2}{\left(\rho_K^{(2e)}(\mathbf{r})\right)^2} - v_s[\rho_{\text{tot}}](\mathbf{r}) + \mu_{\text{tot}}, \tag{72}$$

which provides an analytical expression for $v_{\text{kin}}^{\text{nad}}[\rho_K^{(2e)}, \rho_{\text{tot}}]$ if the potential $v_s[\rho_{\text{tot}}]$ corresponding to the total density is known.

This analytical expression was applied by Savin and Wesołowski[110] to study the exact nonadditive kinetic potential in a four-electron system with the total density $\rho_{\text{tot}} = 2|\psi_{1s}|^2 + 2|\psi_{2s}|^2$, where ψ_{1s} and ψ_{2s} are the 1*s* and 2*s* orbitals of the hydrogen atom. In this case, the corresponding potential is given by $v_s[\rho_{\text{tot}}] = 1/r$. For this simple model system, it is then possible to determine the nonadditive kinetic potential analytically for different partitionings of the total electron density into subsystems. To study more realistic molecular systems, da Silva and Wesołowski subsequently generalized this scheme[111] by choosing the total density as the ground state density obtained from a supermolecular KS-DFT calculation, while still limiting the active subsystem to two electrons. In this case, the effective potential $v_{\text{eff}}[\rho_{\text{tot}}]$ from this supermolecular calculation can be used for $v_s[\rho_{\text{tot}}]$. Note, however, that this is only exact for the exact ground state density.[112] Thus, the use of a finite basis set in the supermolecular KS-DFT calculation introduces a slight inconsistency here.

Such exact reference nonadditive kinetic potentials for analytically solvable cases as well as reference potentials reconstructed numerically (see following section) can be used for analyzing the failure of the

currently available LDA and GGA approximations for covalent bonds between subsystems.[59] The analysis in Ref 59 suggests that the currently available approximations for the nonadditive kinetic potential are not able to distinguish situations in which electrons should be transferred to the frozen subsystem (e.g., in the case of covalent bonds) and situations where this is not the case and the correct long-distance limit should be enforced. To overcome this limitation, it might be promising to develop nondecomposable approximations that make use of the Kohn–Sham orbitals of the subsystems. Finally, it should be mentioned that the limitations of approximate functionals for the nonaddtive kinetic potential can be circumvented by using capping groups.[113] This allows for an efficient treatment of proteins with subsystem DFT.[114]

Reconstructing the Exact Nonadditive Kinetic Potential

So far, we have discussed the calculation of the exact nonadditive kinetic potential for certain special cases. For the general case of an arbitrary number of electrons, $v_s[\rho_K]$ has to be reconstructed numerically. For $v_s[\rho_{\mathrm{tot}}]$, one can either use the potential from a supermolecular KS-DFT calculation or also apply a numerical reconstruction to avoid the inconsistency due to the use of a finite basis set. A large number of algorithms for reconstructing the potential $v_s[\rho_t]$ from a given target density $\rho_t(\mathbf{r})$ have been developed. Conceptually simplest are schemes in which the potential is represented numerically on a real-space grid. In this case, one starts with an initial guess for the potential, usually of the form

$$v_s^{(0)}(\mathbf{r}) = v_{\mathrm{nuc}}(\mathbf{r}) + v_{\mathrm{Coul}}[\rho_t](\mathbf{r}) + v_{\mathrm{FA}}[\rho_t](\mathbf{r}), \qquad (73)$$

where $v_{\mathrm{FA}}[\rho_t](\mathbf{r}) = -(1/n)\int \rho_t(\mathbf{r})/|\mathbf{r}-\mathbf{r}'|\,\mathrm{d}^3r'$ is the Fermi–Amaldi exchange potential, which ensures the correct asymptotic form of the potential,[115] and n is the number of electrons. The potential $v_s[\rho_t]$ is then determined iteratively. In each iteration, one solves the noninteracting Schrödinger equation with the current potential $v_s^{(n)}(\mathbf{r})$ to obtain the corresponding density $\rho^{(n)}(\mathbf{r})$. This density is then compared to the target density at each grid point. If the density $\rho^{(n)}(\mathbf{r})$ is too large, the potential is updated to be more repulsive at this grid point, and if it is too small the potential is made more attractive. This is repeated until convergence is reached. For updating the potential in each iteration, different formulas have been suggested. In the scheme of van Leeuwen and Baerends (LB),[116] the ratio of the density in the current iteration and the target density is used, that is,

$$v_s^{(n+1)}(\mathbf{r}) = \frac{\rho^{(n)}(\mathbf{r})}{\rho_t(\mathbf{r})}\, v_s^{(n)}(\mathbf{r}) \qquad (74)$$

This assumes that the potential is negative at each point, and, therefore, the update formula is usually applied to the exchange–correlation part of the potential only. To reach convergence, it is usually necessary to introduce an additional damping [i.e., a prefactor smaller than one in Eq. (74)] as well as a maximum allowed stepsize at each grid point. An alternative update formula has been suggested by Kadantsev and Stott.[117] It uses the difference between the density in the current iteration and the target density to update the potential as

$$v_s^{(n+1)}(\mathbf{r}) = v_s^{(n)}(\mathbf{r}) + \left[\rho^{(n)}(\mathbf{r}) - \rho_t(\mathbf{r})\right] \qquad (75)$$

Our experience suggests that this scheme often provides a more robust convergence than the original LB scheme. A number of additional schemes for updating the potential at each grid point have also been proposed.[118,119]

An alternative to the LB scheme and its variants is the method of Zhao, Morrison, and Parr (ZMP).[115] Its starting point is the solution of the KS equations under the constraint $\rho(\mathbf{r}) = \rho_t(\mathbf{r})$. This constraint can be implemented by using the potential

$$v_s^{\lambda}(\mathbf{r}) = v_{\mathrm{nuc}}(\mathbf{r}) + \lambda \int \frac{\rho(\mathbf{r}) - \rho_t(\mathbf{r})}{|\mathbf{r}-\mathbf{r}'|}\mathrm{d}\mathbf{r} \qquad (76)$$

and considering the limit $\lambda \to \infty$. In practice, one solves these modified KS equations for several large values of λ and extrapolates to infinity. Even though the ZMP scheme has been used extensively to generate reference exchange–correlation potentials for atoms and small molecules, it turns out to be cumbersome for larger molecules. In particular, it becomes numerically unstable for large values of λ and the need for an extrapolation introduces additional difficulties.[50,120]

More efficient than potential reconstruction algorithms based on a real-space representation of the potential is the expansion of the potential in an auxiliary basis set $\{g_t(\mathbf{r})\}$ as

$$v_s(\mathbf{r}) = v_s^{(0)}(\mathbf{r}) + \sum_t b_t g_t(\mathbf{r}) \qquad (77)$$

Following Wu and Yang (WY),[121,122] the potential yielding the target density can be determined from the unconstrained maximization of the Lagrangian

$$W_s[v_s] = T_s[\{\psi_i\}] + \int v_s(\mathbf{r})[\rho(\mathbf{r}) - \rho_t(\mathbf{r})]\mathrm{d}\mathbf{r} \qquad (78)$$

with respect to the potential, where the KS orbitals $\{\psi_i\}$ are those obtained from the potential $v_s(\mathbf{r})$ and

ρ is the density corresponding to these orbitals. After inserting the basis set expansion of $v_s(\mathbf{r})$, the first and second derivatives of the Lagrangian W_s with respect to the expansion coefficients $\{b_t\}$ can be calculated analytically as[122]

$$\frac{\partial W_s[v_s]}{\partial b_t} = \int \big[\rho(\mathbf{r}) - \rho_t(\mathbf{r})\big] g_t(\mathbf{r}) \mathrm{d}\mathbf{r} \tag{79}$$

and

$$\frac{\partial^2 W_s[v_s]}{\partial b_t \partial b_u} = 4 \sum_i^{\text{occ.}} \sum_a^{\text{virt}} \frac{\langle \psi_i | g_t(\mathbf{r}) | \psi_a \rangle \langle \psi_a | g_u(\mathbf{r}) | \psi_i \rangle}{\epsilon_i - \epsilon_a}, \tag{80}$$

respectively. With this gradient and Hessian available, the maximization of the Lagrangian can be performed using a standard Newton optimization, which usually converges quickly. Note that the grid-based optimization using Eq. (75) corresponds to a steepest-ascent maximization using only the gradient at each grid point.

With all these schemes for reconstructing the potential $v_s[\rho_t]$ that yields a given target density ρ_t, an additional complication arises. If a finite basis set is used for expanding the orbitals when solving the KS equations, the reconstructed potential is not unique,[123,124] that is, different potentials can result in the same density within the finite orbital basis set. To illustrate the origin of this nonuniqueness of the potential, it is instructive to consider the change in the electron density $\Delta\rho(\mathbf{r})$ caused by a change in the potential $\Delta v(\mathbf{r})$. To first order in perturbation theory, one finds

$$\Delta\rho(\mathbf{r}) = 4 \sum_i^{\text{occ.}} \sum_a^{\text{virt}} \frac{\langle \psi_i | \Delta v(\mathbf{r}) | \psi_a \rangle}{\epsilon_i - \epsilon_a} \psi_i(\mathbf{r}) \psi_a(\mathbf{r}). \tag{81}$$

With a finite orbital basis set, the sum over virtual orbitals is truncated. Therefore, there can be changes in the potential $\Delta v(\mathbf{r})$ for which all matrix elements between occupied and virtual orbitals vanish. For such a change in the potential, the density will remain the same. While in this case varying the potential has no effect on the density, it does affect the KS orbitals and their energies. In general (but not necessarily[125]), the different sets of KS orbitals corresponding to identical densities will be related by a unitary transformation.

A number of ways of addressing this ambiguity of the reconstructed potential have been suggested. First, it is possible to obtain a unique potential if the basis sets for the orbitals and for the potential are chosen carefully. In particular, the basis set used for the potential should be such that none of the matrix elements in the numerator of Eq. (81) vanishes. This can be achieved by explicitly constructing potential basis sets that are balanced with respect to a certain orbital basis set[126] or implicitly by discarding potential basis functions that correspond to small singular values of the linear response function entering in Eq. (81).[127] However, choosing the potential basis set to be balanced with respect to the orbital basis set restricts the flexibility available for the potential, which in turn makes the use of very large orbital basis sets necessary. This is a severe obstacle for the routine application of this approach for obtaining the exact embedding potential in subsystem DFT calculations. Moreover, the balancing between orbital and potential basis set will in general be system dependent, because the occupied and virtual orbitals appear in Eq. (81).

An alternative scheme has been developed by Yang and co-workers, who suggested to chose the potential that is as smooth as possible among those that yield the same density. This constraint can be included into the direct optimization of the potential[128] by adding a penalty function to the Lagrangian, that is, by using

$$W_s^{\lambda}[v_s] = T_s[\{\psi_i\}] + \int v_s(\mathbf{r}) \big[\rho(\mathbf{r}) - \rho_t(\mathbf{r})\big] \mathrm{d}\mathbf{r} + \lambda \int |\nabla (v_s(\mathbf{r}) - v_s^{(0)}(\mathbf{r}))|^2 \, \mathrm{d}\mathbf{r} \tag{82}$$

instead of the Lagrangian of Eq. (78). Here, the parameter λ has to be chosen such that the resulting potential is smooth, while the density should still be unchanged.[129] While the requirement that the potential should be smooth is easy to include in the direct optimization of the reconstructed potential, it is, however, not clear whether it leads to the correct potential, that is, whether the potential obtained in the basis set limit should be smooth.

Alternatively, one can employ a two-step procedure that first determines a (nonunique) potential, yielding the target density, for instance via a direct optimization, and subsequently uses the (nonunique) KS orbitals obtained from this potential to single out an unambiguous potential. With the exact KS orbitals, any single KS orbital $\psi_i(\mathbf{r})$ could be used to calculate the corresponding potential—up to a constant shift—as the functional derivative of the von Weizsäcker functional evaluated for the orbital density $\rho_i(\mathbf{r}) = |\psi_i(\mathbf{r})|^2$. Therefore, King and Handy (KH)[130] proposed to calculate the potential as the density-weighted average of the potentials obtained from each single occupied KS orbital (see also Ref 131),

$$v_s^{(KH)}[\{\psi_i\}] = \sum_i^{\text{occ.}} \frac{|\psi_i(\mathbf{r})|^2}{\rho(\mathbf{r})} \left[\frac{\Delta\psi_i(\mathbf{r})}{2\psi_i(\mathbf{r})} + \epsilon_i \right] \tag{83}$$

where the KS orbital energies provide the shifts of the different orbital potentials relative to each other. While this KH potential is exact for the exact orbitals, it is not for those obtained from a nonunique reconstructed potential. In particular, the KH potential is not invariant under unitary transformations of the occupied KS orbitals. Moreover, the density obtained from the KH potential will in general differ from the one corresponding to the orbitals employed to calculate the KH potential. Thus, it does not provide an unambiguous potential, but can nevertheless be used to improve upon the nonunique potential obtained from a potential reconstruction using finite orbital basis sets.

In Ref 131, a related two-step procedure has been proposed. Starting from a nonunique reconstructed potential yielding the target density and the corresponding KS orbitals, one can single out an unambiguous potential by requiring that the target density is still obtained when a complete orbital basis set is used. This potential can be obtained by minimizing

$$\int \frac{1}{\rho(\mathbf{r}')}\left(\sum_{i}^{\text{occ.}}\langle\psi_{\mathbf{r}'}|\hat{T}+v_s|\psi_i\rangle\right)^2 \mathrm{d}\mathbf{r}' \rightarrow \min. \qquad (84)$$

where $\psi_{\mathbf{r}'}(\mathbf{r})$ is an auxiliary basis set for the virtual orbitals, which can be chosen as

$$\psi_{\mathbf{r}'}(\mathbf{r}) = \delta(\mathbf{r}'-\mathbf{r}) - \sum_{j}^{\text{occ.}}\psi_j(\mathbf{r}')\psi_j(\mathbf{r}). \qquad (85)$$

This leads to a linear system of equations for the expansion coefficients of the potential. Here, it is important to note that the above condition is invariant under unitary transformations of the occupied orbitals. Therefore, the resulting potential is unambiguous, that is, it is independent of the outcome of the potential reconstruction in the first step. While the scheme of Ref 131 is not as straightforward as those described earlier, numerical tests indicate that it provides potentials that are very close to the exact ones already with relatively small orbital basis sets,[131,132] which is essential for applying potential reconstruction schemes within subsystem DFT calculations.

Even though with a suitable algorithm for reconstructing the potential that yields a given target density it becomes possible to calculate the exact embedding potential in subsystem DFT, this still requires a supermolecular DFT calculation for the full system. Therefore, such an exact subsystem DFT approach will not provide any computational advantage over a conventional DFT treatment. Nevertheless, such exact subsystem DFT calculations can serve a number of important purposes.

First, the calculation of the exact embedding potential, in particular of its kinetic energy component, can provide important insights for the construction of better approximations for $v_{\text{kin}}^{\text{nad}}[\rho_K, \rho_{\text{tot}}]$. To this end, exact reference potentials have been calculated and analyzed, both for analytically solvable cases[110] and for (molecular) subsystems connected by different types of chemical bonds.[59] While these studies provide some possible directions for future improvements of the approximations for the nonadditive kinetic energy, these have not been developed into generally applicable functionals so far.

Second, one can make the reconstruction of the exact $v_{\text{kin}}^{\text{nad}}[\rho_K, \rho_{\text{tot}}]$ more efficient by exploiting the locality of the interactions between subsystems. This was suggested by Miller and co-workers,[120] who introduced a pair approximation,

$$v_{\text{kin}}^{\text{nad}}[\rho_K, \rho_{\text{tot}}](\mathbf{r}) \approx \sum_I (v_s[\rho_K](\mathbf{r}) - v_s[\rho_K+\rho_I](\mathbf{r})). \qquad (86)$$

This way, the potential reconstruction for the total system is replaced by a potential reconstruction for dimers. This could be further simplified by restricting the summation to subsystems in the neighborhood of the active subsystem K. With such a pair approximation, a treatment of subsystems connected by covalent bonds becomes possible.

Finally, the calculation of the exact embedding potential can be used within generalizations of subsystem DFT for embedding wave function theory (WFT) in DFT. In such calculations, the computational bottleneck is usually the accurate wave function–based calculation for one subsystem of interest, and a conventional DFT calculation of the full system becomes affordable. Such WFT-in-DFT embedding schemes are discussed in more detail in the section Wave Function/DFT-Embedding.

INTERACTION ENERGY CALCULATIONS

The energy of a system in subsystem DFT or FDE can be expressed as a sum of subsystem energies E_I^{sub} plus an interaction energy contribution E^{int},

$$E[\rho_{\text{tot}}] = \sum_I E_I^{\text{sub}}[\rho_I] + E^{\text{int}}[\{\rho_I\}]. \qquad (87)$$

The subsystem energy has the same form as the Kohn–Sham energy expression, but is evaluated with

subsystem orbitals or a subsystem density,

$$E_I^{\mathrm{sub}}[\rho_I] = T_s[\{\psi_{i_I}\}] + V_{\mathrm{nuc}}^{(I)}[\rho_I] + J[\rho_I] + E_{\mathrm{xc}}[\rho_I] + V_{\mathrm{nn}}^{(I)}. \quad (88)$$

The interaction energy in the context of subsystem DFT is then defined as

$$E^{\mathrm{int}}[\{\rho_I\}] = T_s^{\mathrm{nad}}[\{\rho_I\}] + E_{\mathrm{xc}}^{\mathrm{nad}}[\{\rho_I\}] + \sum_{I\neq J} V_{\mathrm{nuc}}^{(I)}[\rho_J] + \sum_{I<J} J[\rho_I, \rho_J] + \sum_{I<J} V_{\mathrm{nn}}^{IJ} \quad (89)$$

where $E_{\mathrm{xc}}^{\mathrm{nad}}[\{\rho_I\}]$ is defined in analogy to $T_s^{\mathrm{nad}}[\{\rho_I\}]$ as

$$E_{\mathrm{xc}}^{\mathrm{nad}}[\{\rho_I\}] = E_{\mathrm{xc}}[\rho_{\mathrm{tot}}] - \sum_I E_{\mathrm{xc}}[\rho_I], \quad (90)$$

and the Coulomb interaction energy $J[\rho_I, \rho_J]$ is given as

$$J[\rho_I, \rho_J] = \int \frac{\rho_I(\mathbf{r})\rho_J(\mathbf{r}')}{|\mathbf{r}-\mathbf{r}'|}\mathrm{d}\mathbf{r}\mathrm{d}\mathbf{r}'. \quad (91)$$

The nucleus–nucleus interaction energy between two subsystems is simply,

$$V_{\mathrm{nn}}^{IJ} = \sum_{A\in I}\sum_{B\in J} \frac{Z_A Z_B}{|\mathbf{R}_A - \mathbf{R}_B|} \quad (92)$$

and $V_{\mathrm{nuc}}^{(I)}[\rho_J]$ represents the electrostatic attraction between the nuclei of system I and the electron density ρ_J,

$$V_{\mathrm{nuc}}^{(I)}[\rho_J] = -\sum_{A\in I}\int \rho_J(\mathbf{r})\frac{Z_A}{|\mathbf{R}_A - \mathbf{r}|}\mathrm{d}\mathbf{r} \quad (93)$$

One should keep in mind that the true interaction energy between different subsystems is usually defined in a different way, namely as the difference in energies of the total system (e.g., a complex of molecules; $E[\rho_{\mathrm{tot}}]$) and the sum of energies of its separate, *isolated* constituting fragments,

$$E^{\mathrm{int}'} = E[\rho_{\mathrm{tot}}] - \sum_I E_I^{\mathrm{sub,iso}}\left[\rho_I^{\mathrm{iso}}\right]. \quad (94)$$

Hence, this true interaction energy contains additional effects, namely (i) structural rearrangements between isolated subsystems and subsystems in the complex (indicated by the usage of the symbol $E_I^{\mathrm{sub,iso}}$), and (ii), even if structural differences are neglected, a possible polarization in the electron density. To fully compare subsystem DFT results with those of KS-DFT, one thus also has to compare how well equilibrium structures are represented and how well the electron densities of the interacting subsystems are reproduced by subsystem DFT (see the section *Calculation of Charge Densities and Multipole Moments*).

The subsystem DFT interaction energy denoted as $E^{\mathrm{int}}[\{\rho_I\}]$ above, in contrast, only contains the interaction energy terms of prearranged subsystem electron densities as appearing in the complex. In cases where both structural and polarization effects are negligible, for example, for interacting rare gas atoms, the two definitions of interaction energies will coincide. In the following, we will give an overview over studies investigating interaction energies for several classes of interacting subsystems.

Choice of the Nonadditive Kinetic Energy Functional

The accuracy of interaction energies from subsystem DFT (relative to KS-DFT) depends on two main issues: First, the density of the total system must be described correctly, which necessitates an accurate embedding potential and thus an accurate functional derivative of the nonadditive kinetic energy. Second, also the parent nonadditive kinetic energy functional must be of sufficient accuracy. The analysis of the accuracy of a certain consistent approximation for nonadditive kinetic energy and potential is of course complicated by the fact that error cancellation effects may take place, which mask deficiencies in the potential by errors in the energy functional with opposing effect. Studies of the accuracy of electron densities from subsystem DFT have already been discussed in the section *Calculation of Charge Densities and Multipole Moments*, and we will give an overview over tests concentrating on interaction energies in the following after a few general remarks.

As far as weak interactions are concerned, we first observe that the electrostatic interaction between different subsystems is described exactly for a given electron density distribution in subsystem DFT, just like in KS-DFT. Also the electrostatic potential is included exactly in self-consistent subsystem DFT. Hence, the mutual polarization of the subsystems (taken isolated subsystem densities as a reference) is fully captured, at least as far as electrostatic terms are concerned. This is in contrast to, for example, QM/MM embedding schemes, in which electrostatic terms are often expressed in terms of multipole expansions of the electrostatic potential. For the exchange–correlation potential, typically the same approximations can be used as in KS-DFT, so that also short-range quantum mechanical polarization effects due to exchange and correlation are described in the same way as in KS-DFT. The only difference in the potential, and thus in the density change, may arise from approximations in the nonadditive kinetic

energy functional. This, in turn, can also lead to errors in the electrostatic interaction energy.

For nonoverlapping subsystem densities, that is, $\rho_1(\mathbf{r})\rho_2(\mathbf{r}) = 0$ for every point $\mathbf{r}$, the nonadditive exchange–correlation and nonadditive kinetic energy contributions from LDA- and GGA-type approximations are zero. Hence, the asymptotic $-(C/R^6)$ distance dependence known for London dispersion forces cannot be reproduced correctly by subsystem DFT relying on this type of approximation, as was already observed by Senatore and Subbaswamy.[14] Possible solution strategies are the same as those used for Kohn–Sham DFT,[133] although special care should be taken in regions of small density overlap, where subsystem DFT shows a different behavior than Kohn–Sham DFT due to the approximations in $T_s^{\mathrm{nad}}[\{\rho_I\}]$. Nevertheless, one can adopt the point of view that subsystem DFT is a well-defined approximation to KS-DFT and that empirical dispersion corrections used for the latter can be used in the same way in subsystem DFT calculations, as their only purpose is to correct problems in the exchange–correlation energy. This has been tried and combined with a subsystem-DFT based energy decomposition analysis by Visscher and co-workers.[134]

Extensive studies of different nonadditive kinetic energy functionals have been carried out in self-consistent subsystem DFT calculations. Wesołowski and co-workers conducted a large number of tests for weakly interacting systems, for example, hydrogen-bonded complexes,[89,92] van der Waals complexes,[60,135,136] the physisorption of H_2 on polycyclic aromatic hydrocarbons,[137] and π-stacked systems.[138] A systematic comparison of LDA and GGA-type nonadditive kinetic energy functionals was presented in Ref 40, where it was found that GGA-type functionals significantly improve interaction energies for complexes with larger density overlap. LDA was found to predict very good interaction energies for weakly overlapping densities, as for example for rare gas dimers. The most important finding of these early studies on interaction energies are summarized in the review in Ref 22. In particular, it was observed that interaction energies from subsystem DFT were consistently better than the corresponding Kohn–Sham DFT interaction energies for weakly bound complexes when comparing to accurate wave function–based calculations.[40] In that study, the error in the interaction energy was also analyzed in terms of zeroth- and first-order energy contributions when expanding the error as a functional of the density change upon complexation. The error in electrostatic interaction terms was not considered in that expression, which was justified by their analytically known forms. However, the density change upon complexation of course depends on the approximations in the potential derived from the kinetic energy functional and leads to changes in the electrostatic energy contributions. The analysis in Refs 22,40 must thus be considered to be limited to those cases in which no significant errors are introduced into the density change upon complexation by employing an approximate nonadditive kinetic energy potential.

Based on extensive tests, a nonadditive kinetic energy functional derived from the PW91 exchange functional[67] and reparameterized for the kinetic energy by Lembarki and Chermette[68] was recommended by Wesołowski in 1997.[89] This functional is often called PW91k or LC94 as mentioned in the section *Decomposable Approximations for the Nonadditive Kinetic Potential*, though the term "GGA97" has been introduced later[56,139] to highlight the difference between a *kinetic-energy* approximation and a *nonadditive kinetic energy* approximation. The acronym GGA97 is only used for the latter, following the recommendations for nonadditive kinetic energy functionals in Refs 89,92.

A comparative study of KS and subsystem DFT using the test sets established by Zhao and Truhlar[140,141] was conducted in Ref 91. This study showed that a consistent LDA approximation for the nonadditive kinetic energy and exchange–correlation functionals worked best among all electronic-structure methods tested for weakly interacting complexes, and was still very good for hydrogen-bonded complexes (see also Ref 142) and dipolar interacting systems. It was found to be less well suited for π-stacking interactions and charge-transfer systems. GGA functionals for the nonadditive kinetic energy contributions showed reasonably good results for hydrogen bonding, charge-transfer, and dipolar interactions, whereas they were found to be much worse for the weakly interacting systems. A recent test including also more strongly interacting compounds demonstrated, however, that within the class of GGA kinetic energy functionals, none is of much better accuracy than and thus preferable over the others.[143] For zinc coordination compounds, surprisingly good interaction energies were reported for DGE-derived functionals in that study, even though the absolute errors are still rather disappointing for such strongly interacting systems. Della Sala and co-workers have conducted a benchmark study in which they compared the accuracy of several nonadditive kinetic energy functionals derived from PBE and compared them to KS-DFT.[80] On the basis of this study, they concluded that the quality of the results depends on the balance of the enhancement factor for

regions of low and high reduced density gradients, and they recommended the nonempirical revAPBEK functional for nonbonded interactions. This group also presented a study within the generalized Kohn–Sham context, employing the localized Hartree–Fock exchange functional as well as nonlocal hybrid functionals, and reported energies comparable to or better than those obtained with semilocal approximations.[30]

Besides this large number of benchmark applications, in particular the Warshel group has carried out studies where FDE and/or subsystem DFT were employed in larger scale calculations, for example, on proton transfer in aqueous solution[97] or assisted by a metal complex,[144] on the autodissociation of water,[145] and on the reduction potential of redox proteins.[146] In the latter case, FDE was used as an alternative to QM/MM treatments to increase the quantum mechanical region. A completely different field has been investigated by Trail and Bird,[147] who have implemented FDE in a plane wave context. They studied the energy and density of bulk fcc aluminum, in which one cubic sublattice of aluminum atoms was embedded in three other sublattices. The best results in that case were obtained with a nonlocal approximation for the nonadditive kinetic energy. Energy levels and other properties of solids have also been studied by Boyer and co-workers in a series of articles on the basis of a so-called *self-consistent atomic deformation* method, which can be regarded as a variant of subsystem DFT.[148–153] Another related method has been used by Zhang and co-workers in studies of bulk metals.[154–156]

Overall, it can be concluded from the tests of subsystem DFT for interaction energies that this method is usually quite good and often better than KS-DFT even with highly parameterized functionals for weakly interacting systems. However, the errors are usually quite system dependent, so that caution is required when applying them to quantify interactions between subsystems.

FDE as a Constrained DFT Variant

In the limit of an exact functional $T_s^{\mathrm{nad}}[\{\rho_I\}]$ and an exact treatment of the corresponding contribution to the potential, FDE and subsystem DFT would become equivalent to KS-DFT (provided the representability conditions are met). This also means that they would suffer from the same deficiencies as observed in KS-DFT calculations which arise from the necessity to use approximate exchange–correlation energy functionals and potentials.

A particularly interesting aspect of FDE calculations is that some of these deficiencies, most notably the overdelocalization problem arising from the self-interaction error in KS-DFT,[12,51] can actually be avoided if standard approximations for T_s^{nad} and its functional derivatives are employed. It clearly has to be stated that this is a case of error cancellation effect, but with very fortunate practical consequences. One reason is that the standard approximations in the potential are often too repulsive in the vicinity of (but not directly at) the nuclei of the environmental system (see, e.g., the examples in Ref 59). This together with the fact that embedding calculations are usually carried out (i) using only a monomer basis set and (ii) starting from the properties of the isolated system, often allows to introduce specific constraints into DFT calculations. Furthermore, a certain partitioning and an assignment of a certain number of electrons to each fragment has to be provided by the user, which again can introduce specific restrictions to a calculation.

As an example, consider the case of an S_N2 reaction of the type,

$$X^- + CH_3Y \longrightarrow XCH_3 + Y^-.$$

From a quantum mechanical point of view, nothing but the geometric assembly of the nuclei has changed in the system: The number of nuclei, their charges, and the number of electrons stay the same during the reaction. However, we can also think of this reaction in a more chemical way, describing the left-hand side by a (quasi)diabatic state with the characteristics of the CH_3Y molecule and an approaching X^- ion. In contrast, the right-hand side can be characterized by a (quasi)diabatic state consisting of the XCH_3 molecule and a leaving Y^- ion. At a certain point along the reaction coordinate, the two diabatic states will cross. In a subsystem DFT or FDE calculation using approximate functionals, we can actually choose one of the two diabatic representations by assigning the corresponding nuclei and electrons to one of the subsystems. In this way, diabatic potential energy surfaces can be generated. Warshel and co-workers have used this possibility for modeling nucleophilic substitution reactions in solution and parameterized an effective empirical valence bond Hamiltonian on the basis of FDE calculations.[157] Similarly, they studied proton transfer reactions in solution.[158] For the use of subsystem DFT and FDE in connection with the empirical valence bond approach, see also the review by Kamerlin and Warshel[159]; note that FDE (with a completely frozen environmental density) is denoted as "frozen DFT" (FDFT) in that review, whereas the relaxed variant including freeze-and-thaw cycles (subsystem DFT) is dubbed "constrained DFT" (CDFT). The expression "CDFT" is, however, in the context of DFT usually used in a broader

context and often refers to calculations in which an explicit constraining potential is incorporated into the KS equations.[160] Two typical applications of this type of CDFT are calculations on charge- and spin-localized states in DFT. Without such constraints, DFT calculations on charged and open-shell systems often suffer from an overdelocalization problem due to the self-interaction error. It has recently been demonstrated that FDE can, in a similar spirit, be employed to generate diabatic states and couplings for charge-[161] and spin-localized states,[51] thus pragmatically overcoming some of the limitations of Kohn–Sham DFT with conventional approximations. In fact, a recent study demonstrated that highly accurate charge-transfer excitation energies can be obtained from this type of calculations.[162]

PROPERTY AND SPECTRA CALCULATIONS

Many molecular properties are strongly influenced by a surrounding medium. Among the most prominent examples are solvent effects on molecular spectra such as UV/vis, fluorescence, infrared, electron spin resonance, and nuclear magnetic resonance spectra.[163] But also more complex environmental and/or aggregation effects can change the properties of molecules, for example, when arranged on surfaces, in crystals, or in biological environments such as proteins. This has triggered a large activity in the quantum chemistry community to develop environmental models for electronic-structure calculations.[6] Subsystem DFT and FDE are ideally suited to describe environmental effects, as the properties of a subsystem are calculated under the influence of an explicit surrounding represented in electronic-structure detail and taking into account all quantum mechanical interactions. In fact, the original papers on subsystem DFT were aiming at molecular properties, such as the in-crystal polarizabilities of rare gas atoms,[14] from which dielectric constants can be estimated, or structural and cohesive properties of ionic crystals.[16] Cortona already mentions the applicability to molecular systems,[16] and the initial FDE work by Wesołowski and Warshel specifically addresses solvated systems.[17] It is thus not very surprising that a large activity has occurred in the field of molecular property and spectra calculations on the basis of FDE and subsystem DFT. Previous overviews have been given in Refs 22, 23. The following sections will thus concentrate on the most recent work.

One additional remark should be made here, however. From a purist's point of view, the individual subsystems, theirs densities and orbitals are just auxiliary quantities in the subsystem-DFT calculation, and what should be interpreted are only the results for the total system. However, because we usually start from an intuitive isolated subsystem perspective, the changes in a subsystem density and the corresponding properties (e.g., a dipole moment) are typically interpreted as changes in the properties of that particular molecule or fragment. That this can be misleading is easily demonstrated for a Bader charge analysis[164]: The density formally associated with subsystem *A* can extend to regions in space that belong to the atomic basin of an atomic nucleus of a different subsystem. Hence, Bader charges derived from a subsystem density will be different from those obtained in Bader analysis of the total density, which is the proper way.[31,95] The same problem occurs for Mulliken charges if a supermolecular basis is employed, but not if a monomer expansion is used.

Structural Parameters and Dynamics

There have been several studies in which structural parameters of chemical systems have been determined on the basis of subsystem DFT and FDE. Several investigations addressed systems with only one or a few degrees of freedom, for example, the metal–ligand distance in transition metal complexes.[165] A basic computational requirement for efficient investigations on the structure and dynamics of general molecular systems is the availability of analytic energy-gradient implementations. A first gradient implementation in the deMon package[166] was mentioned and used in a study of CO adsorbed on zeolite in 2001,[167] though only very few technical details were given there. A systematic study of structures obtained with LDA and GGA approximations in the context of subsystem DFT calculations was conducted later by Dułak et al.[168] This study used test cases from Refs 140, 141, and the results supported the findings of earlier studies: LDA for the nonadditive kinetic energy gave favorable results for hydrogen-bonding complexes and other weakly bound systems, whereas a GGA functional did not lead to significant improvements. Only for complexes involving interactions with π systems, the GGA-type nonadditive kinetic energy approximation was found more suitable.

Molecular dynamics (MD) simulations based on forces from subsystem DFT have been conducted by Iannuzzi et al. in 2006.[169] They reported "consistently longer and weaker hydrogen bonds" than with the corresponding Kohn–Sham methods, and "no signature of a second solvation shell." A related, yet simplified dynamics was presented by Hodak et al.[170] These authors used fixed solvent electron densities in

molecular dynamics simulations, while the density of an active system was optimized via FDE-like equations. Another method related to subsystem DFT was presented by Shimojo et al.,[171] who performed a study on CdSe with a focus on parallelization and scalability issues of their "embedded divide-and-conquer" algorithm. This algorithm has later also been used for MD studies on energetic nanocomposite materials.[172]

NMR and ESR Properties, Spin Densities

One of the present authors has presented a subsystem DFT generalization for nuclear magnetic resonance (NMR) shieldings[173] and employed it for calculations on acetonitrile–solvent complexes. An assumption that is implied in these calculations is that not only the density but also the current density of the total system can be partitioned into subsystem contributions. Absolute accuracies of the solvent-induced shifts in the nitrogen shieldings of about 2 ppm could be achieved in comparison to KS-DFT reference results. Aspects of NMR shielding calculations in the context of a multilevel setup have been discussed in Ref 101. In a later extension, a conformational sampling was carried out, which indicated a significant dependence on the type of molecular dynamics simulation used for the sampling.[174]

Another field of application of FDE and subsystem DFT are spin-dependent properties. The KSCED equations can straightforwardly be extended to the spin-polarized case (see, e.g., Refs 41, 50, 161). Wesołowski applied the spin-dependent FDE and subsystem DFT formalisms to investigate the effect of rare gas matrices on the hyperfine coupling constants of Mg^+,[175] and found a good agreement with experimental data. This study was subsequently extended to hyperfine coupling constants of alkali metal atoms in charge-transfer complexes with CO_2,[49] in which the subsystems are much more strongly interacting. In the case of $LiCO_2$ and $NaCO_2$, again a good agreement was observed both with experiment and with KS-DFT results. For the case of potassium, however, the (spin-)density changes induced by the carbon dioxide subsystem were found to be too strong to be described correctly on the basis of the PW91k functional employed. Later on, solvent effects on the ^{14}N and ^{1}H hyperfine coupling constants were modeled based on conformational samplings[176] and demonstrated the usefulness of FDE in this context. Subsystem DFT is in principle capable of modeling spin-polarization in closed-shell systems through nearby open-shell systems, though this effect was found to be negligible in a test in Ref 176. Apart from hyperfine coupling constants, also isotropic *g*-values have been studied with subsystem DFT. In Ref 177, models for a biliverdin radical in a complex with a phycocyanobilin:ferredoxin oxidoreductase protein were studied. These models comprised three or five amino acids. This study concentrated mostly on technical details of the calculation, and indicated that also isotropic *g*-values can be strongly affected if large basis sets are used in connection with Coulombic-only embedding.

A study of spin-density distributions from FDE was recently reported in Ref 51. This study clearly demonstrated the ability to describe spin-polarization of formally closed-shell fragments in terms of spin-subsystem DFT, which is interesting for studies of solvated radicals. The results showed that the spin-polarization effect is not generally negligible. This approach was then also used to study spin-polarization effects in a model for the special pair radical cation in photosynthetic reaction center complexes of purple bacteria. This special pair is a dimer of (bacterio)chlorophyll molecules located at the top of a chain of electron donors/acceptors arranged in two branches of approximate C_2 symmetry. Interestingly, only one of the two branches is active in the photosynthetic charge transport.[178–180] It was shown by an investigation of the spin populations that histidines directly bound to the special pair reduce the difference in spin polarization in the two halves of the special pair radical cation, while an inclusion of a larger part of the environment actually increases this asymmetry again.

Excited States, Electronic Spectra, and Response Properties

Modeling environmental effects on excited electronic states and electronic spectra is one of the most important fields of application of subsystem and embedding schemes. It is thus not surprising that FDE and subsystem DFT have been used as explicit models for solvatochromism and general environmental effects on optical spectra. In first studies on excited states, ligand-field splitting parameters were extracted from orbital energy differences of metal complexes, for example, lanthanide–halide clusters in elpasolite crystals,[181,182] or MnF_6^{4-} complexes in fluoroperovskites.[165] A discussion of the relation of simpler ligand field splitting methods to FDE can be found in Ref 183.

Another simple pragmatic way of obtaining excited states of an active subsystem in an environment is to perform a ΔSCF-DFT calculation, in which the environment is represented in terms of a density-dependent embedding potential. FDE has been used to estimate singlet–triplet splittings in a study on the

mechanism of nitrate reduction, which can be regarded as a ΔSCF-DFT type calculation.[139]

The most widely used approach for excitation energies in DFT is time-dependent density functional (response) theory, TDDFT. A response variant of subsystem DFT was developed by Casida and Wesołowski in 2004.[184] The underlying idea is to express the response in the electron density to a time-dependent external field as a sum of subsystem contributions. For the Fourier components of the density change at a certain angular frequency ω, we thus write,

$$\delta\rho(\mathbf{r},\omega) = \delta\rho_A(\mathbf{r},\omega) + \delta\rho_B(\mathbf{r},\omega). \tag{95}$$

In KS-TDDFT, the density response is determined through the linear-response equation (the frequency dependence will be dropped for brevity in the following),[23,185–190]

$$\delta\rho(\mathbf{r}) = \int \chi_s(\mathbf{r},\mathbf{r}')\delta v_{\text{eff}}(\mathbf{r}')\mathrm{d}\mathbf{r}', \tag{96}$$

where

$$\chi_s(\mathbf{r},\mathbf{r}') = \frac{\delta\rho(\mathbf{r})}{\delta v_{\text{eff}}(\mathbf{r}')}, \tag{97}$$

is the single-particle response function. The change in the potential, $\delta v_{\text{eff}}(\mathbf{r})$, contains the applied external field $\delta v_{\text{ext}}(\mathbf{r})$ and a part induced by the density change, which is expanded to first order in the density change, $\delta v_{\text{ind}}(\mathbf{r})$,

$$\delta v_{\text{eff}}(\mathbf{r}) = \delta v_{\text{ext}}(\mathbf{r}) + \delta v_{\text{ind}}(\mathbf{r}) \tag{98}$$

$$= \delta v_{\text{ext}}(\mathbf{r}) + \int f(\mathbf{r},\mathbf{r}')\delta\rho(\mathbf{r}')\mathrm{d}\mathbf{r}', \tag{99}$$

with the kernel,

$$f(\mathbf{r},\mathbf{r}') = \frac{\delta v_{\text{eff}}(\mathbf{r})}{\delta\rho(\mathbf{r}')} = \frac{1}{|\mathbf{r}-\mathbf{r}'|} + f_{\text{xc}}(\mathbf{r},\mathbf{r}'), \tag{100}$$

where f_{xc} is the so-called exchange–correlation kernel. Usually, the adiabatic approximation is made here and the exchange–correlation kernel is evaluated as a frequency-independent second functional derivative of the ground state exchange–correlation energy functional E_{xc}. In a symbolic notation, the density change can be rewritten as[184]

$$\delta\rho = \chi_s(\delta v_{\text{ext}} + f\delta\rho), \tag{101}$$

where actually two integrations are involved on the right-hand side. In this symbolic form, the equation can be rewritten as

$$(\chi_s^{-1} - f)\delta\rho = \delta v_{\text{ext}} \tag{102}$$

From this equation, one can determine the excitation energies of the system as resonance frequencies of $(\chi_s^{-1} - f)$, that is, as frequencies for which the density change becomes infinite even for a vanishingly small external perturbation δv_{ext}. This problem can be cast into an eigenvalue equation for the (squares of the) excitation energies.

Casida and Wesołowski have derived, in a similar spirit, a symbolic expression for the corresponding operator of subsystem A in a supersystem consisting of two fragments, $[(\chi_s^A)^{-1} - f_{\text{eff}}^A)]$, and pointed out that it is enough to determine the explicit form of the kernel if also the orbitals and orbital energies of subsystem A are known, which determine χ_s^A.[184] The symbolic form of the effective kernel for subsystem A given in their work contains the response function of the other subsystem, thus showing that the responses of the two subsystems are, of course, coupled. Shortly after, Wesołowski implemented a simplified version of this subsystem-based response theory, in which it is explicitly assumed that the response contribution from the environment (subsystem B) is zero.[191] This case, later called "uncoupled FDE" (FDEu)[192] or "neglect of dynamic response of the environment" (NDRE),[193] may be regarded as a strict FDE-TDDFT variant, in which the environmental density is considered frozen also in the response framework. The corresponding response equation looks like that of the isolated system A, only that the orbitals and orbital energies are obtained under the influence of the effective embedding potential given in Eq. (27), and instead of the kernel for the isolated system A,

$$f_{\text{iso}}^A(\mathbf{r},\mathbf{r}') = \frac{1}{|\mathbf{r}-\mathbf{r}'|} + \frac{\delta^2 E_{\text{xc}}[\rho_A]}{\delta\rho_A(\mathbf{r}')\delta\rho_A(\mathbf{r})} \tag{103}$$

we have to use an effective kernel,

$$f_{\text{eff}}^A(\mathbf{r},\mathbf{r}') = \frac{\delta v_{\text{eff}}^{(A)}(\mathbf{r})}{\delta\rho_A(\mathbf{r}')} + \frac{\delta v_{\text{emb}}^{(A)}(\mathbf{r})}{\delta\rho_A(\mathbf{r}')} \tag{104}$$

$$= \frac{1}{|\mathbf{r}-\mathbf{r}'|} + \frac{\delta^2 E_{\text{xc}}[\rho_A+\rho_B]}{\delta\rho_{\text{A}}(\mathbf{r}')\delta\rho_{\text{A}}(\mathbf{r})} + \frac{\delta^2 T_s^{\text{nad}}[\rho_A,\rho_B]}{\delta\rho_A(\mathbf{r}')\delta\rho_A(\mathbf{r})}. \tag{105}$$

In 2007, one of the present authors derived a generalization of subsystem TDDFT for an arbitrary number of subsystems, in which the effect of the density change of all subsystems is explicitly taken into account in a coupled manner.[192] The induced potential in a certain subsystem K is then expressed as,

$$\delta v_{\text{ind}}^{(K)}(\mathbf{r}) = \sum_I \int \left(\frac{\delta v_{\text{eff}}^{(K)}(\mathbf{r})}{\delta\rho_I(\mathbf{r}')} + \frac{\delta v_{\text{emb}}^{(K)}(\mathbf{r})}{\delta\rho_I(\mathbf{r}')} \right) \delta\rho_I(\mathbf{r}')\mathrm{d}\mathbf{r}', \tag{106}$$

Since this approach allows to calculate excitations which are delocalized over several subsystems and which can be considered as excitonically coupled monomer excitations,[194] this method is also denoted as coupled FDE or FDEc for excited states (referring to FDE in a more general sense). This subsystem TDDFT formalism has been rederived recently (i) with an emphasis on the similarity to Hartree–Fock based approaches, which also allowed to introduce the Tamm–Dancoff approximation[195] and (ii) yielding Dyson-type equations that allow to distinguish coupled and uncoupled response functions.[196]

As far as excited-state applications of FDE- and subsystem-TDDFT are concerned, we have to distinguish between two common types. In the first type, the system of interest is a chromophore embedded in a larger environment, for example, a solvent, a protein, or a crystal. In this case, the FDEu approximation is typically working well, since the excitation can be assumed to be localized, although there may be a certain polarization of the environment in response to the excitation. The second type concerns systems with several interacting chromophores, for example, aggregates of dyes. The interaction between the dyes can lead to significant changes in the electronic spectra and cannot be described in terms of changes of local transitions alone. Here, the FDEc approach has to be employed.[3,10,23,197] We would also like to note that in excited-state applications, a strict distinction between subsystem DFT and FDE is even more difficult than in ground state applications. The reason is that the variational optimization of electron densities in the ground state and inclusion of (approximate) response can be chosen independently for the subsystems in practice.

The first investigations of excited states with FDE and subsystem DFT were all restricted to the FDEu approximation for local excitations. A pilot study on nucleic acid dimers showed that hydrogen-bonding induced shifts in excitation energies can reliably be reproduced by FDEu.[191] Since the local excitations on the different monomers have rather similar excitation energies, this case was reinvestigated later, lifting the uncoupled approximation.[197] It was confirmed that the excitation energies from FDEu are already quite good, but exciton-like interactions between the local transitions can lead to a mixing in character and to a redistribution of oscillator strengths. Additional investigations demonstrated for the examples of solvated acetone[198] and aminocoumarin C151[199] that the FDEu approximation can successfully be used as an explicit quantum chemical solvation model. This work mostly concentrated on possible improvements of the efficiency by employing simplified environmental densities if a large number of molecular dynamics snapshots of the solvated chromophore shall be investigated. In particular, the superposition of densities of individual solvent molecules for (outer) solvation shells was tested. A recent study along the same lines used an even more approximate, yet more efficient setup of the environmental electron density of a zeolite by superimposing spherical atomic densities.[200] This facilitated the investigation of several hundred MD snapshots of the fluorenone chromophore in zeolite L. A comparison of FDEu and a polarizable classical force field for excitation energies showed that the classical model is still computationally much less demanding, but predicted smaller solvent-induced shifts, most probably due to an incomplete description of short-range effects.[98] Another comparison of an acetone–water complex demonstrated that FDEu nicely reproduces the distance dependence of the hydrogen-bond induced shift in the $n \rightarrow \pi^*$ excitation energy of acetone, and that a neglect of the non-classical contributions in the embedding potential would lead to an increased mismatch with the supermolecular TDDFT results.[201] In contrast to that, a significant offset of the excited-state potential energy curve was observed with the polarizable classical model if no system-specific reparameterization was carried out.

FDEu can be preferable over conventional TDDFT calculations for large systems not only in terms of efficiency but also because the latter can lead to a large number of (at least partially) spurious excited states, which are absent in FDE calculations. This was shown for solvated molecules, where intermolecular charge-transfer excitations may affect the interpretation,[198] for organic host–guest complexes suffering from similar problems,[202] and for molecules adsorbed to surfaces,[201] where bulk transitions can hamper the assignment of valence excitations of the adsorbate.

The necessity to average over a large number of snapshots from an MD simulation for obtaining accurate results is one of the drawbacks of explicit solvent models as far as their efficiency is concerned. In contrast to that, implicit solvent models implicitly contain such an averaging over the solvent degrees of freedom.[6,203] An attempt to combine the advantages of the electron-density–based FDE embedding potential with such an implicit inclusion of different solvent conformations was presented by Kaminski et al.[39] To evaluate the solvent effect on excitation energies, the environmental density was constructed based on statistically mechanically averaged site distribution for the solvent derived from the so-called three-dimensional (3D) reference

interacting site model with the Kovalenko–Hirata closure approximation (3D-RISM-KH).[204] Good results were observed in comparison to explicitly averaged solvation studies as well as to the implicit conductor-like screening model.[205] The key assumption in this 3D-RISM-KH–based model is thus that instead of averaging over several excitation energy calculations obtained with different embedding potentials, one can employ one single embedding potential with a statistically averaged environmental electron density. Another successful application of this method was presented by Zhou et al.[206] for the solvatochromic shift of coumarin 153 in nine different solvents, thus underlining that FDE can, with a few additional assumptions, also be employed as a competitive implicit solvent model.

Several studies investigated hydrogen-bond–induced shifts in excitation energies. Fradelos et al. demonstrated that the effect of an increasing number of solvent molecules in microsolvated *cis*-7-hydroxyquinoline is highly non-additive.[193] For the same chromophore, it was later shown that solvatochromic shifts induced by hydrogen bonds are actually better described by FDEu than by supermolecular TDDFT calculations, taking equation-of-motion coupled cluster (EOM-CC) calculations as a reference.[53] Interestingly, it was found there that nonrelaxed solvent densities lead to better agreement with the EOM-CC results than densities relaxed by freeze-and-thaw cycles. This study was extended by Fradelos et al. in Ref 207, where additional details of the EOM-CC and FDEu approach were investigated. In yet another study on this chromophore, Fradelos and Wesołowski later also demonstrated that erroneous solvatochromic shifts may be obtained if only the Coulomb contribution to the effective embedding potential is employed.[47] This is, however, typically only the case with large basis sets, where the electrons have the variational freedom to probe regions of space belonging to the frozen environment, where most approximations to the effective embedding potential show an incorrect behavior.[59,94,95,102,109]

In addition to the calculation of excitation energies and UV–vis absorption spectra, FDEu was also employed in a study on induced circular dichroism (ICD)[202]. This study showed that, on the one hand, FDEu can reliably predict ICD effects due to hydrogen bonding or complexation in crown ether moieties. On the other hand, however, it indicated for the first time a clear failure of the uncoupled approximation for the case of a phenol molecule in a host–guest complex with a β-cyclodextrin. Through an additional comparison of FDEu and supermolecular calculations for a benzaldehyde dimer, it could clearly be shown in that work that the FDEu approximation breaks down for excitonically coupled chromophores, in which excitations delocalized over several molecules occur, which can be understood as linear combinations of local excitations.

The subsystem TDDFT (or FDEc) approach developed in Ref 192 solves this problem and provides a very powerful method for the investigation of chromophore aggregates embedded in complex environments. An important field of application is photosynthetic light-harvesting complexes, which can contain a large number of pigments such as different chlorophyll derivatives, bilins, and carotenoids.[3] Consequently, subsystem TDDFT has been employed to study the local transition energies, excitonic couplings, and possible energy transfer pathways derived from these data for the light-harvesting complex II (LHII) of purple bacteria,[194] the light-harvesting complex II (LHCII) of green plants,[208] and the Fenna–Matthews-Olson (FMO) complex of green sulfur bacteria.[209] The latter calculations addressed almost the entire protein–pigment complex in a fully quantum-chemical fashion, treating more than 7000 atoms. A picture of this complex containing the site energies and the most important excitonic couplings obtained from the largest structural model of the FMO protein is shown in Figure 5. An important result gained from the investigations in Ref 209 is that the site energies employed in model theories for excitation energy transfer are very sensitive to the setup of the structural model, whereas the exciton couplings appear to be much more stable against such variations. Apart from calculations in the context of photosynthesis, also the spectroscopy of astaxanthin in crustacyanin proteins was investigated with FDEc.[210] There, it could be shown on the basis of absorption and circular dichroism spectra that exciton couplings are qualitatively not suited to explain the observed color change upon release of astaxanthin from the protein. Reviews over subsystem-based applications in biomolecular spectroscopy in general and photosynthetic systems in particular are provided in Refs 3, 10.

The work in Ref 192 has made it possible to address entirely new classes of problems on the basis of subsystem DFT. For example, the question of differential polarization effects by the environment on solvatochromic effects could be studied. In Ref 197, several earlier calculations without this effect were repeated including the coupling to excited states of the environment. It could be shown that in particular for microsolvation studies, the effect was typically rather small. In the context of excitonically coupled dyes, the response of a solvent can lead to a change in the

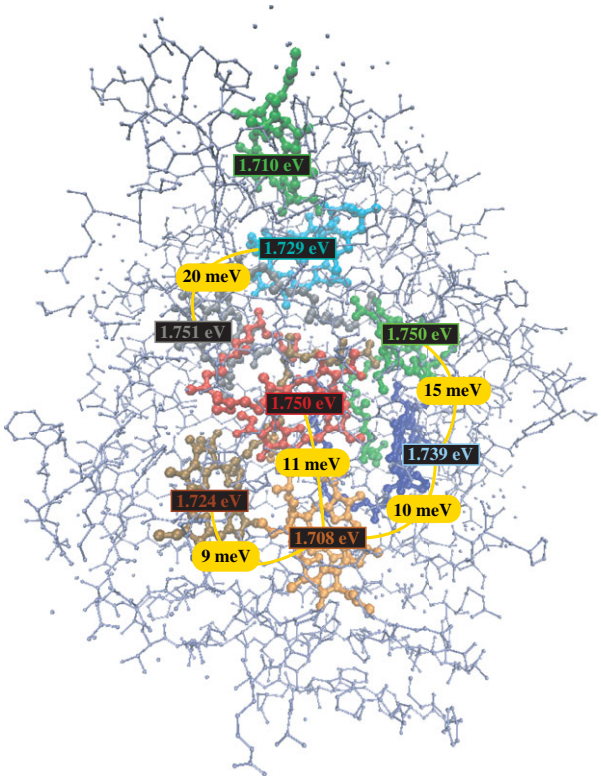

FIGURE 5 | Structure of the model for the FMO complex (>7000 atoms), site energies of the bacteriochlorophyll subsystems, and most important excitonic couplings obtained in Ref 209.

exciton splitting. Also this can be modeled with FDEc, as has been shown in Ref 211. Since this requires an explicit coupling to many excited states of the solvent, that work also introduced additional algorithmic improvements to select and couple selectively those excited states which can be expected to have the highest impact on differential polarization. Two additional subsequent developments are (i) the re-derivation and implementation of subsystem TDDFT within the Tamm–Dancoff approximation to TDDFT,[195] which can be advantageous in studies involving carotenoids, and (ii) the combination of hybrid functionals for local excitations with a nonhybrid treatment of exciton interactions to distinguish direct from indirect exchange- (or Dexter-)type couplings.[212]

The response formalism formulated by Casida and Wesołowski[184] can in principle also be extended for calculations of frequency-dependent response properties. Within the local response (FDEu or NDRE) approximation, this was tested for the first time in Ref 98 and compared to finite field calculations and calculations using a polarizable force-field method. The results for polarizabilities were, however, rather disappointing and must be traced back to the neglect of the response of the environment. Again, a coupled response treatment is necessary, which was developed in explicit form in Ref 213. This led to much better agreement of polarizabilities and also of optical rotatory dispersion with reference results from supermolecular Kohn–Sham response theory in systems with induced chirality. This is an important prerequisite if "unusual" solvent effects in chiroptical spectroscopy shall be described, like chiral imprinting effects.[214,215] Since the solvent plays an active (and even dominant) role in these effects, subsystem DFT offers a unique possibility as a solvent model in such cases.

WAVE FUNCTION/DFT-EMBEDDING

In subsystem DFT, as described in the preceding sections, all subsystems are treated using approximate exchange–correlation functionals. However, one of the advantages of subsystem approaches is the possibility to selectively employ more accurate wave function–based methods (wave function theory, WFT) for only a few subsystems. The fact that subsystem DFT uses only the electron density, which is available in any quantum-chemical method, to take the interaction between the subsystems into account makes it particularly easy to set up such WFT-in-DFT embedding schemes (for previous reviews, see Refs 216,217).

As a starting point, one can use the expression for the total energy in subsystem DFT [Eq. (24)] and replace the terms referring to subsystem K by those provided by a wave function–based description,[218,219]

$$E[\Psi_K, \{\rho_I\}_{I\neq K}] = \langle \Psi_K | \hat{T} + \hat{V}_{\text{ext}}^K + \hat{V}_{ee} | \Psi_K \rangle + V_{\text{nn}}^K + \sum_{I\neq K} E_I^{\text{sub}}[\rho_I] + E_{\text{int}}[\{\rho_I\}]. \tag{107}$$

Here, one keeps the evaluation of the interaction energy using DFT, and the wave function–based description of subsystem K enters the interaction energy only via its density $\rho_K(\mathbf{r})$. As long as all density functionals are assumed to be exact, this energy expression is also exact.

To determine the wave function Ψ_K of subsystem K, one minimizes the above energy expression. This leads to an embedded Schrödinger equation for subsystem K,[217,219]

$$\left[\hat{T} + \hat{V}_{\text{ext}}^K + \hat{V}_{ee} + \hat{V}_{\text{emb}}^K[\rho_K, \{\rho_I\}]\right] \Psi_K = E'_K \Psi_K \tag{108}$$

in which the interaction with all other subsystems enters as an embedding operator

$$\hat{V}^K_{\text{emb}}[\rho_K, \{\rho_I\}] = \sum_i v_{\text{emb}}[\rho_K, \{\rho_I\}](\mathbf{r}_i), \qquad (109)$$

where $v_{\text{emb}}[\rho_K, \{\rho_I\}](\mathbf{r}_i)$ is the embedding potential that is also present in subsystem DFT [Eq. (27)]. The embedded Schrödinger equation for subsystem K can now be solved using any (approximate) quantum-chemical method. Note, however, that the energy eigenvalue E'_K contains part of the interaction energy, and thus differs from the energy of subsystem K as defined previously.

The original formulation of WFT-in-DFT outlined here (and also the acronym itself) can be understood as a hybrid energy scheme, in which the energy for the active system is calculated on the basis of WFT, whereas the energy of the surroundings and the interaction energy are obtained from DFT. A strict formal derivation of WFT-in-DFT embedding within the theoretical framework of DFT has been given by Wesołowski.[35] In this derivation, all density functionals are considered exact, whereas the wave function is obtained from a truncated expansion, that is, it is considered as only approximate. In this case, an additional correction term that accounts for the error in the wave function arises in the embedding potential. However, there is no way to account for this correction in practical calculations.[220] Moreover, in general the DFT treatment of the environment will introduce larger errors than the wave function–based calculation for a selected subsystem. Consequently, it is difficult to see the advantages of introducing such a correction term when applying WFT-in-DFT embedding schemes in practice. Note that another generalization that concerns an embedded system described by a one-particle reduced density matrix has been derived by Pernal and Wesołowski.[38]

WFT-in-DFT embedding schemes based on subsystem-DFT have been first proposed by Carter and co-workers for studying atoms and molecules adsorbed on metallic surfaces.[221,222] In this situation, WFT-in-DFT calculations can be used to improve the periodic DFT description by using WFT for a smaller cluster consisting of the adsorbate and a small part of the surface. To have a WFT density available, it is necessary to employ quantum-chemical methods for which the electron density can be calculated easily and efficiently. For this reason, configuration interaction (CI) and complete active space self-consistent field (CASSCF) have mainly been used in WFT-in-DFT embedding calculations so far.

The application of WFT-in-DFT to adsorbates on surfaces faces additional difficulties when defining the subsystems and when attempting to update the subsystem densities self-consistently. The active subsystem K should be chosen as a cluster consisting of the adsorbate and a small part of the surface. Thus, the complementary frozen subsystem would consist of the periodic surface, from which some atoms have been removed. This results in a system with unsaturated valances and treating such an isolated frozen subsystem appropriately is difficult. To overcome this problem, in their initial setup,[218,219,221,222] Carter and co-workers used a periodic DFT calculation to determine the total density ρ_{tot}. This total density is then kept fixed, and the frozen density is obtained as $\rho_B = \rho_{\text{tot}} - \rho_{\text{WFT}}$.

While such a setup does not require calculations on an unphysical system for obtaining the frozen density, it becomes more difficult to update the frozen density self-consistently. A number of schemes have been developed to provide a possibility to determine the densities of all subsystems iteratively.[223,224] Recently, Carter and co-workers proposed a potential-functional embedding approach, in which the minimization with respect to the subsystem densities is replaced by a minimization with respect to the (unique) embedding potential.[225] Such a formulation provides a conceptually simple way to determine the densities of all subsystems self-consistently.

One important application of WFT-in-DFT embedding schemes is the description of local electronic excitations, for instance of molecules adsorbed on surfaces, of impurities in solids, or of solvated molecules. Here, one has to distinguish between state-specific WFT excited-state methods, in which a different wave function is calculated for each electronic state, and methods based on response theory, which calculate the linear response of the ground state wave function to a time-dependent external perturbation. For the case of state-specific WFT methods, the formal theory has been derived by Khait and Hoffmann,[226] whereas Höfener et al. considered the case of WFT methods based on response theory[227] using the theoretical framework of the quasi-energy formalism.[228] For a comprehensive review, we refer to Ref 217.

The simplest approach for applying WFT-in-DFT embedding to excited states neglects the response of the frozen environment to the electronic excitation in the active subsystem, which corresponds to the FDEu scheme outlined above. In this approximation, the same frozen density is used for all excited states. With state-specific WFT methods for the active subsystem, the embedding potential for different electronic states n only differs because different densities $\rho_K^{(n)}$ enter when evaluating the

embedding potential. This approach has been applied to study the local excited states of CO on a Pt(111) surface[221,222] and of local excited states in MgO[229] using CI and CASSCF for the active subsystem. With response methods, the dependence of the embedding potential on the density of the active subsystem enters via an embedding contribution to the response kernel in analogy to Eq. (105). This approach has been tested for the local excitations of a water molecules inside a cluster of 127 water molecules using TDHF for the active subsystem.[227]

For modeling local excitations with WFT-in-DFT, it is often possible to apply additional approximations. In many cases, one can neglect the contribution arising from the dependence of the embedding potential on the density of the active subsystem[230] and use the same ground state embedding potential for all electronic states. This approximation is justified by the observation that the additional embedding contribution to the response kernel is usually small.[98] Moreover, in many cases DFT already provides an accurate ground state density and WFT is only necessary to overcome the difficulties of TDDFT in describing certain types of excitations. Therefore, it has been suggested to determine the embedding potential in a conventional subsystem-DFT calculation and to use this fixed embedding potential in a subsequent WFT-in-DFT calculation of local excited states.[230] This simplified scheme has been assessed for acetone solvated in water, using coupled-cluster response theory (CC2) for the acetone subsystem, and has been applied to model the excited states of the neptunyl ion embedded as impurity into a $Cs_2UO_2Cl_4$ crystal with Fock-space coupled cluster theory.

On the other hand, it is also possible to set up WFT-in-DFT embedding schemes for excited states that include the response of the environment. With state-specific WFT methods, this is possible by iteratively updating the densities of all subsystems in freeze-and-thaw iterations for each electronic state.[226] However, such an approach can be computationally demanding and leads to excited-state wave functions for the active subsystem that are not orthogonal to the ground state (and to each other), which complicates the calculation of transition moments. Recently, a first study employing approximate state-specific embedding potentials based on DFT-derived ground and excited state densities of the active system has been presented,[231] which explicitly allows to include differential polarization effects. With excited-state WFT methods based on response theory, an alternative theory can be derived,[227] which is analogous to the FDEc approach outlined above for subsystem-DFT. While working equations have been derived for coupled-cluster response theory, an implementation or applications of such a coupled scheme have not been presented yet. This would allow for the efficient inclusion of the polarization of the environment as well as the calculation of exciton couplings with WFT-in-DFT, which could further be generalized to a WFT description for all or several subsystems (WFT-in-WFT embedding.[232])

In the applications of WFT-in-DFT embedding schemes discussed so far, the kinetic energy contribution to the embedding potential has been calculated using approximate functionals, but exact WFT-in-DFT embedding schemes using potential reconstruction methods have also been developed recently. For WFT-in-DFT embedding the full, supermolecular DFT calculation required for the reconstruction of the embedding potential is not a computational bottleneck anymore because the accurate WFT calculation for the active subsystem is usually more expensive. This was first realized by Roncero et al.,[233] who devised a variant of the simplified WFT-in-DFT scheme of Ref 230 using an embedding potential reconstructed from a partitioning of the density from a supermolecular calculation. Such a partitioning can either be obtained by using localized orbitals[233] or can be determined iteratively in freeze-and-thaw iterations.[234]

In a similar fashion, Miller and co-workers devised a fully self-consistent subsystem-DFT method using the reconstructed embedding potential,[120] and recently extended their work to WFT-in-DFT embedding.[235] In contrast to Roncero et al., the scheme of Miller and co-workers does not use the embedding potential from a subsystem-DFT calculation, but the density from the WFT calculation is used when reconstructing the embedding potential. Thus, this scheme presents the first fully self-consistent WFT-in-DFT scheme using an accurate reconstructed embedding potential. It has been demonstrated that this scheme can be employed to treat covalent bonds between the active subsystem and its environment. Moreover, this scheme has been extended to open shell systems to allow for the treatment of transition metal complexes. For a $Fe(H_2O)^{2+}$ complex (in which the central iron ion forms the active subsystem treated with CASSCF whereas the water ligands constitute the environment treated with DFT), it was shown that such WFT-in-DFT schemes can be used to overcome the deficiencies of standard exchange–correlation functionals in predicting the energy difference between the high-spin and the low-spin states. Finally, we note that also the potential-functional embedding theory approach of Carter and co-workers[225] provides a conceptually simple and flexible method

for fully self-consistent WFT-in-DFT embedding calculations using the exact embedding potential.

The results of such "exact" WFT-in-DFT embedding calculations will depend sensitively on the choice of the method for the potential reconstruction. Here, the nonuniqueness of the reconstructed embedding potential will affect the outcome of the WFT calculation for the active subsystem, even though the same density would be obtained in a DFT calculation. In the works of Roncero et al. the ZMP method was used for the potential reconstruction, and the nonuniqueness of the reconstructed embedding potential was not addressed further.[233,234] Initially, Miller and co-workers also employed the ZMP scheme,[50,235] but switched to the direct optimization of WY in combination with a smoothness constraint in their subsequent work.[235] To regularize the reconstructed embedding potential, they further calculate the KH potential in a second step from the reconstructed orbitals. Carter and co-workers[41,225] also used the direct optimization of WY in combination with a smoothness constraint, but employed the resulting potentials directly. As discussed above, none of these reconstruction methods provides a truly unambiguous potential in finite basis sets, and the consequences of this shortcoming for the results of the corresponding WFT-in-DFT calculations will have to be explored in more detail in future work.

CONCLUSIONS AND OUTLOOK

In this review we have shown that subsystem DFT in its different variants is one of the most appealing strategies to describe large chemical systems based on first principles. It can be regarded as an exact variant of DFT in the limit of exact functionals, provided the corresponding representability conditions are met. By focusing on one or a few selected subsystems, the frozen-density embedding method as well as WFT-in-DFT embedding schemes emerge naturally from subsystem DFT. The interactions between the subsystems can be described without recourse to system-specific parameters, which is an advantage over other hybrid methods such as QM/MM,[45,46] ONIOM,[236] or the fragment molecular orbital method,[237,238] even though these methods are certainly very successful in practice. Another advantage over QM/MM methods is the fact that the (often dominant) electrostatic contribution of the environment is represented exactly for a given density in the embedding potential arising in subsystem DFT, and that short-range quantum mechanical effects are also incorporated. The latter are in particular important to avoid spurious charge leaking in cases of large, diffuse basis sets. The ability to represent spin-dependent environmental potentials is a further important aspect of subsystem DFT calculations.

The extensions of subsystem DFT and FDE for molecular property calculations are diverse, and often offer great advantages over the corresponding KS calculations. In contrast to other environmental models, response contributions of a surrounding medium can be incorporated into the calculation, and even cases in which the response of several (or many) subsystems needs to be included explicitly can easily be handled. This gives access to calculations of, for example, aggregates of excitonically coupled chromophores, or to unusual solvent effects which are dominated by the solvent rather than the solute. If solvent response contributions are less important, statistically mechanically averaging for the construction of the environmental density in an FDE calculation can greatly enhance the efficiency and establish a connection to implicit models for environmental effects.

Density-dependent approximations for the nonadditive kinetic energy functional and its functional derivatives often work well for weakly interacting systems. For stronger interactions (ranging up to covalent bonds), one can resort to potential reconstruction techniques, which make it possible to set up formally "exact" embedding schemes. In practice, there is no significant computational saving in such a calculation, but potentials obtained in this way are important references for the development of new approximate embedding potentials. Furthermore, and maybe even more important, such potentials can be transferred to WFT-in-DFT embedding, so that highly correlated wave function methods can be combined with DFT descriptions of those parts of a molecule which can be treated with lower accuracy in a given context. We believe that using such methods in applications to subsystems treated with highly accurate wave function methods, which are embedded in a larger environment described in terms of DFT, is currently one of the most promising directions for high-accuracy quantum chemical descriptions of complex systems.

ACKNOWLEDGMENTS

J.N. is supported by a VIDI grant (700.59.422) of the Netherlands Organisation for Scientific Research (NWO). C.R.J. acknowledges funding from the DFG-Center for Functional

Nanostructures. We also acknowledge support from COST Action CODECS. We thank Carolin König for preparing Figure 5, and Michele Pavanello as well as Tomasz A. Wesołowski for helpful discussions.

REFERENCES

1. Gordon MS, Fedorov DG, Pruitt SR, Slipchenko LV. Fragmentation Methods: A Route to Accurate Calculations on Large Systems. *Chem Rev* 2012, 112:632–672.
2. VandeVondele J, Borštnik U, Hutter J. Linear Scaling Self-Consistent Field Calculations with Millions of Atoms in the Condensed Phase. *J Chem Theory Comput* 2012, 8:3563–3573.
3. König C, Neugebauer J. Quantum Chemical Description of Absorption Properties and Excited-State Processes in Photosynthetic Systems. *Chem Phys Chem* 2012, 13:386–425.
4. Senn H-M, Thiel W. QM/MM Methods for Biological Systems. *Top Curr Chem* 2007, 268:173–290.
5. Chung LW, Hirao H, Li X, Morokuma K. The ONIOM method: its foundation and applications to metalloenzymes and photobiology. *WIREs Comput Mol Sci* 2012, 2:327–350.
6. Mennucci B, Cammi R, eds. *Continuum Solvation Models in Chemical Physics: From Theory to Applications*. New York: Wiley; 2007.
7. Gordon MS, Freitag MA, Bandyopadhyay P, Jensen JH, Kairys V, Stevens WJ. The Effective Fragment Potential Method: A QM-Based MM Approach to Modeling Environmental Effects in Chemistry. *J Phys Chem A* 2001, 105:293–307.
8. Kobayashi M, Nakai H. Extension of linear-scaling divide-and-conquer-based correlation method to coupled cluster theory with singles and doubles excitations. *J Chem Phys* 2008, 129:044103.
9. Haag MP, Reiher M. Real-Time Quantum Chemistry. *Int J Quantum Chem* 2013, 113:8–20.
10. Neugebauer J. Subsystem–based theoretical spectroscopy of biomolecules and biomolecular assemblies. *Chem Phys Chem* 2009, 10:3148–3173.
11. Jensen F. *Introduction to Computational Chemistry*. 2nd ed. Chichester: Wiley; 2007.
12. Cramer CJ. *Essentials of Computational Chemistry*. 2nd ed. Chichester: Wiley; 2004.
13. Yang W. Direct Calculation of Electron Density in Density-Functional Theory. *Phys Rev Lett* 1991, 66:1438–1441.
14. Senatore G, Subbaswamy KR. Density dependence of the dielectric constant of rare-gas crystals. *Phys Rev B* 1986, 34:5754–5757.
15. Johnson MD, Subbaswamy KR, Senatore G. Hyperpolarizabilities of alkali halide crystals using the local-density approximation. *Phys Rev B* 1987, 36:9202–9211.
16. Cortona P. Self-consistently determined properties of solids without band-structure calculations. *Phys Rev B* 1991, 44:8454–8458.
17. Wesolowski TA, Warshel A. Frozen Density Functional Approach for *ab Initio* Calculations of Solvated Molecules. *J Phys Chem* 1993, 97:8050–8053.
18. Parr RG, Yang W. *Density-Functional Theory of Atoms and Molecules*. Oxford: Oxford University Press; 1989.
19. Engel E, Dreizler RM. *Density Functional Theory*. Heidelberg: Springer; 2011.
20. Levy M. Universal variational functionals of electron densities, first-order density matrices, and natural spin-orbitals and solution of the v-representability problem. *Proc Natl Acad Sci USA* 1979, 76:6062–6065.
21. Perdew JP, Parr RG, Levy M, Balduz JL Jr. Density-Functional Theory for Fractional Particle Number: Derivative Discontinuities of the Energy. *Phys Rev Lett* 1982, 49:1691.
22. Wesolowski TA. One-electron equations for embedded electron density: challenge for theory and practical payoffs in multi-level modeling of complex polyatomic systems. In: Leszczynski J, ed. *Computational Chemistry: Reviews of Current Trends*, vol 10, Singapore: World Scientific; 2006, 1–82.
23. Neugebauer J. Chromophore-specific theoretical spectroscopy: From subsystem density functional theory to mode-specific vibrational spectroscopy. *Phys Rep* 2010, 489(1-3):1–87.
24. Wesolowski TA, Wang YA, eds. *Recent Progress in Orbital-Free Density Functional Theory*. Singapore: World Scientific; 2013.
25. Gordon RG, Kim YS. Theory for the Forces between Closed-Shell Atoms and Molecules. *J Chem Phys* 1972, 56:3122.
26. Kim YS, Gordon RG. Study of the electron gas approximation. *J Chem Phys* 1974, 60:1842.
27. Gombas P. *Die statistische Theorie des Atoms und ihre Anwendungen*. Wien: Springer; 1949.
28. Laricchia S, Fabiano E, Della Salla F. Frozen density Embedding with Hybrid Functionals. *J Chem Phys* 2010, 133:164111.
29. Laricchia S, Fabiano E, Della Salla F. Frozen Density Embedding Calculations with the Orbital-Dependent Localized Hartree–Fock Kohn–Sham Potential. *Chem Phys Lett* 2011, 518:114–118.
30. Laricchia S, Fabiano E, Della Salla F. On the accuracy of frozen density embedding calculations with hybrid

and orbital-dependent functionals for non-bonded interaction energies. *J Chem Phys* 2012, 137:014102.

31. Kiewisch K, Eickerling G, Reiher M, Neugebauer J. Topological analysis of electron densities from Kohn–Sham and subsystem density functional theory. *J Chem Phys* 2008, 128:044114.
32. Wesolowski TA, Weber J. Kohn-Sham equations with constrained electron density: an iterative evaluation of the ground-state electron density of interacting molecules. *Chem Phys Lett* 1996, 248:71–76.
33. Gritsenko OV, Visscher L. Density-orbital embedding theory. *Phys Rev A* 2010, 82:032519.
34. Gritsenko O. On the principal difference between the exact and approximate frozen-density embedding theory. In: Wesolowski TA, Wang YA, eds. *Recent Progress in Orbital-Free Density Functional Theory*, Singapore: World Scientific; 2013, 357–370.
35. Wesolowski TA. Embedding a multideterminantal wave function in an orbital-free environement. *Phys Rev A* 2008, 77:012504.
36. Wesolowski TA, Savin A. Non-additive kinetic energy and potential in analytically solvable systems and their approximated counterparts. In: Wesolowski TA, Wang YA, eds. *Recent Progress in Orbital-Free Density Functional Theory*. Singapore: World Scientific; 2013, 275–295.
37. See the preface to Ref [24].
38. Pernal K, Wesołowski TA. Orbital-Free Effective Embedding Potential: Density-Matrix Functional Theory Case. *Int J Quantum Chem* 2009, 109:2520–2525.
39. Kaminski JW, Gusarov S, Wesołowski TA, Kovalenko A. Modeling Solvatochromic Shifts Using the Orbital-Free Embedding Potential at Statistically Mechanically Averaged Solvent Density. *J Phys Chem A* 2010, 114:6082–6096.
40. Wesolowski TA, Tran F. Gradient-free and gradient-dependent approximations in the total energy bifunctional for weakly overlapping electron densities. *J Chem Phys* 2003, 118:2072.
41. Huang C, Pavone M, Carter EA. Quantum mechanical embedding theory based on a unique embedding potential. *J Chem Phys* 2011, 134:154110.
42. Elliot P, Cohen MH, Burke K, Wasserman A. Density Functional Partition Theory with Fractional Occupations. *J Chem Theory Comput* 2009, 5:827–833.
43. Elliot P, Burke K, Cohen MH, Wasserman A. Partition density-functional theory. *Phys Rev A* 2010, 82:024501.
44. Cohen MH, Wasserman A. On Hardness and Electronegativity Equalization in Chemical Reactivity Theory. *J Stat Phys* 2006, 125:1121–1139.
45. Warshel A, Levitt M. Theoretical studies of enzymic reactions: Dielectric, electrostatic and steric stabilization of the carbonium ion in the reaction of lysozyme. *J Mol Biol* 1976, 103:227-249.
46. Senn HM, Thiel W. QM/MM Methods for Biomolecular Systems. *Angew Chem, Int Ed* 2009, 48:1198–1229.
47. Fradelos G, Wesolowski TA. Importance of the Intermolecular Pauli Repulsion in Embedding Calculations for Molecular Properties: The Case of Excitation Energies for a Chromophore in Hydrogen-Bonded Environments. *J Phys Chem A* 2011, 115:10018–10026.
48. Jacob Ch R, Reiher M. Spin in density-functional theory. *Int J Quantum Chem* 2012, 112:3661–3684.
49. Wesołowski TA, Weber J. Spin-densities in charge-transfer complexes derived from DFT calculations using an orbital-free embedding scheme for interacting subsystems. In: Barone V, Bencini A, Fantucci P, eds. *Recent Advances in Density Functional Methods Part III*. Singapore: World Scientific; 2002, 371–386.
50. Goodpaster JD, Ananth N, Manby FR, Miller TF III. Exact nonadditive kinetic potentials for embedded density functional theory. *J Chem Phys* 2010, 133:084103.
51. Solovyeva A, Pavanello M, Neugebauer J. Spin Densities from Subsystem Density-Functional Theory: Assessment and Application to a Photosynthetic Reaction Center Complex Model. *J Chem Phys* 2012, 136:194104.
52. Laio A, VandeVondele J, Rothlisberger U. A Hamiltonian electrostatic coupling scheme for hybrid Car–Parrinello molecular dynamics simulations. *J Chem Phys* 2002, 116:6941–6947.
53. Fradelos G, Lutz JJ, Wesołowski TA, Piecuch P, Włoch M. Embedding vs Supermolecular Strategies in Evaluating the Hydrogen-Bonding-Induced Shifts of Excitation Energies. *J Chem Theory Comput* 2011, 7:1647–1666.
54. Stefanovich EV, Truong TN. Embedded density functional approach for calculations of adsorption on ionic crystals. *J Chem Phys* 1996, 104:2946–2955.
55. Jacob Ch R, Wesolowski TA, Visscher L. Orbital-free embedding applied to the calculation of induced dipole moments in $CO_2 \cdots X$ (X=He, Ne, Ar, Kr, Xe, Hg) van der Waals complexes. *J Chem Phys* 2005, 123:174104.
56. Dulak M, Wesolowski TA. On the electron leak problem in orbital-free embedding calculations. *J Chem Phys* 2006, 124:164101.
57. Wesolowski TA. Exact inequality involving the kinetic energy functional $T_s[\rho]$ and pairs of electron densities. *J Phys A: Math Gen* 2003, 36:10607–10613.
58. Manby FR, Stella M, Goodpaster JD, Miller TF III. A Simple, Exact Density-Functional-Theory Embedding Scheme. *J Chem Theory Comput* 2012, 8:2564–2568.
59. Fux S, Jacob Ch R, Neugebauer J, Visscher L, Reiher M. Accurate frozen-density embedding potentials as a

first step towards a subsystem description of covalent bonds. *J Chem Phys* 2010, 132:164101.

60. Wesolowski TA, Morgantini P-Y, Weber J. Intermolecular interaction energies from the total energy bifunctional: A case study of carbazole complexes. *J Chem Phys* 2002, 116:6411–6421.
61. Wang YA, Carter EA. Orbital-free kinetic-energy density functional theory. In: Schwartz SD, ed. *Theoretical Methods in Condensed Phase Chemistry*. Dordrecht: Kluwer; 2000, 117–184.
62. Dreizler RM, Gross EKU. *Density Functional Theory — An Approach to the Quantum Many-Body Problem*. Berlin: Springer; 1990.
63. Hodges CH. Quantum Corrections to the Thomas–Fermi Approximation — The Kirzhnits Method. *Can J Phys* 1973, 51:1428–1437.
64. Lee H, Lee C, Parr RG. Conjugate gradient correction to the Hartree–Fock kinetic- and exchange-energy density functionals. *Phys Rev A* 1991, 44:768–771.
65. March NH, Santamaria R. Non-Local Relation Between Kinetic and Exchange Energy Densities in Hartree–Fock Theory. *Int J Quantum Chem* 1991, 39:585–592.
66. Becke AD. Density-functional exchange-energy approximation with correct asymptotic behavior. *Phys Rev A* 1988, 38:3098–3100.
67. Perdew JP. Unified Theory of Exchange and Correlation Beyond the Local Density Approximation. In: Ziesche P, Eschrig H, eds. *Electronic Structure of Solids '91*. Berlin: Akademie Verlag; 1991, 11–20.
68. Lembarki A, Chermette H. Obtaining a gradient-corrected kinetic-energy functional from the Perdew-Wang exchange functional. *Phys Rev A* 1994, 50:5328.
69. Tran F, Wesolowski TA. Semilocal approximations for the kinetic energy. In: Wesolowski TA, Wang YA, eds. *Recent Progress in Orbital-Free Density Functional Theory*. Singapore: World Scientific; 2013, 429–442.
70. Thomas LA. The calculation of atomic fields. *Proc Camb Phil Soc* 1927, 23:542–548.
71. Fermi E. Eine statistische Methode zur Bestimmung einiger Eigenschaften des Atoms und ihre Anwendung auf die Theorie des periodischen Systems der Elemente. *Z Phys* 1928, 48:73–79.
72. von Weizsäcker CF. Zur Theorie der Kernmassen. *Z Phys* 1935, 96:431–458.
73. Lee D, Constantin LA, Perdew JP, Burke K. Condition on the Kohn–Sham kinetic energy and modern parametrization of the Thomas–Fermi density. *J Chem Phys* 2009, 130:034107.
74. Ou-Yang H, Levy M. Approximate Noninteracting Kinetic Energy Functionals from a Nonuniform Scaling Requirement. *Int J Quantum Chem* 1991, 40:379–388.
75. Lacks DJ, Gordon RG. Tests of nonlocal kinetic energy functionals. *J Chem Phys* 1994, 100:4446–4452.
76. Tran F, Wesolowski TA. Link between the Kinetic- and Exchange-Energy Functionals in the Generalized Gradient Approximation. *Int J Quantum Chem* 2002, 89:441–446.
77. Thakkar AJ. Comparison of kinetic-energy density functionals. *Phys Rev A* 1992, 46:6920–6924.
78. Karasiev VV, Trickey SB, Harris FE. Born–Oppenheimer interatomic forces from simple, local kinetic energy density functionals. *J Compu-Aid Mat Des* 2006, 13:111–129.
79. Constantin LA, Fabiano E, Laricchia S, Sala FD. Semiclassical Neutral Atom as a Reference System in Density Functional Theory. *Phys Rev Lett* 2011, 106:186406.
80. Laricchia S, Fabiano E, Constantin L, Sala FD. Generalized Gradient Approximation of the Noninteracting Kinetic Energy from the Semiclassical Atom Theory: Rationalization of the Accuracy of the Frozen Density Embedding Theory for Nonbonded Interactions. *J Chem Theory Comput* 2011, 7:2439–2451.
81. Wang YA, Govind N, Carter EA. Orbital-free kinetic-energy functionals for the nearly free electron gas [Errata: Phys. Rev. B **60** (1998), 17162; Phys. Rev. B **64** (2001), 129901]. *Phys Rev B* 1998, 58:13465–13471.
82. Choly N, Kaxiras E. Kinetic energy density functionals for non-periodic systems. *Sol State Commun* 2002, 121:281–286.
83. García-Aldea D, Alvarellos JE. Fully nonlocal kinetic energy density functionals: A proposal and a general assessment for atomic systems. *J Chem Phys* 2008, 129:074103.
84. Karasiev VV, Trickey SB. Issues and challenges in orbital-free density functional calculations. *Comput Phys Commun* 2012, 183:2519–2527.
85. Huang C, Carter EA. Nonlocal orbital-free kinetic energy density functional for semiconductors. *Phys Rev B* 2010, 81:045206.
86. Xia J, Huang C, Shin I, Carter EA. Can orbital-free density functional theory simulate molecules. *J Chem Phys* 2012, 136:084102.
87. Oliver GL, Perdew JP. Spin-density gradient expansion for the kinetic energy. *Phys Rev A* 1979, 20:397–403.
88. Scuseria GE, Staroverov VN. Progress in the development of exchange–correlation functionals. In: Dykstra CE, Frenking G, Kim KS, Scuseria GE, eds. *Theory and Applications of Computational Chemistry: The First Forty Years*. Amsterdam: Elsevier; 2005, 669–724.
89. Wesolowski TA. Density functional theory with approximate kinetic energy functionals applied to hydrogen bonds. *J Chem Phys* 1997, 106:8516–8526.

90. Dulak M, Wesolowski TA. The Basis Set Effect on the Results of the Minimization of the Total Energy Bifunctional $E[\rho_A, \rho_B]$. *Int J Quantum Chem* 2005, 101:543–549.
91. Dułak M, Wesołowski TA. Interaction energies in non-covalently bound intermolecular complexes derived using the subsystem formulation of density functional theory. *J Mol Model* 2007, 13:631–642.
92. Wesolowski TA, Chermette H, Weber J. Accuracy of approximate kinetic energy functionals in the model of Kohn-Sham equations with constrained electron density: The FH···NCH complex as a test case. *J Chem Phys* 1996, 105:9182.
93. Wesolowski TA, Weber J. Kohn–Sham Equations with Constrained Electron Density: The Effect of Various Kinetic Energy Functional Parametrizations on the Ground-State Molecular Properties. *Int J Quantum Chem* 1997, 61:303.
94. García-Lastra JM, Kaminski JW, Wesolowski TA. Orbital-free effective embedding potential at nuclear cusps. *J Chem Phys* 2008, 129:074107.
95. Fux S, Kiewisch K, Jacob Ch R, Neugebauer J, Reiher M. Analysis of electron density distributions from subsystem density functional theory applied to coordination bonds. *Chem Phys Lett* 2008, 461:353–359.
96. Beyhan SM, Götz AW, Jacob Ch R, Visscher L. The weak covalent bond in NgAuF (Ng=Ar, Kr, Xe): A challenge for subsystem density functional theory. *J Chem Phys* 2010, 132:044114.
97. Wesolowski T, Warshel A. Ab Initio Free Energy Perturbation Calculations of Solvation Free Energy Using the Frozen Density Functional Approach. *J Phys Chem* 1994, 98:5183–5187.
98. Jacob Ch R, Jensen L, Neugebauer J, Visscher L. Comparison of frozen-density embedding and discrete reaction field solvent models for molecular properties. *Phys Chem Chem Phys* 2006, 8:2349–2359.
99. Amsterdam density functional program. Theoretical Chemistry, Vrije Universiteit, Amsterdam. URL: http://www.scm.com. (Accessed January 1, 2013).
100. te Velde G, Bickelhaupt FM, Baerends EJ, van Gisbergen SJA, Fonseca Guerra C, Snijders JG, Ziegler T. Chemistry with ADF. *J Comput Chem* 2001, 22:931–967.
101. Jacob Ch R, Neugebauer J, Visscher L. A flexible implementation of frozen-density embedding for use in multilevel simulations. *J Comput Chem* 2008, 29:1011–1018.
102. Jacob Ch R, Beyhan SM, Visscher L. Exact functional derivative of the nonadditive kinetic-energy bifunctional in the long-distance limit. *J Chem Phys* 2007, 126:234116.
103. Jacob Ch R, Visscher L. Towards the description of covalent bonds in subsystem density-functional theory. In: Wesolowski TA, Wang YA, eds. *Recent Progress in Orbital-Free Density Functional Theory*. Singapore: World Scientific; 2013, 299–324.
104. Gritsenko OV, Schipper PRT, Baerends EJ. Approximation of the exchange–correlation Kohn–Sham potential with a statistical average of different orbital model potentials. *Chem Phys Let* 1999, 302:199–207.
105. Gritsenko OV, Schipper PRT, Baerends EJ. Ensuring Proper Short-Range and Asymptotic Behavior of the Exchange–Correlation Kohn–Sham potential by Modeling with a Statistical Average of Different Orbital Model Potentials. *Int J Quantum Chem* 2000, 76:407–419.
106. Schipper PRT, Gritsenko OV, van Gisbergen SJA, Baerends EJ. Molecular calculations of excitation energies and (hyper)polarizabilities with a statistical average of orbital model exchange–correlation potentials. *J Chem Phys* 2000, 112:1344–1352.
107. Liu S, Ayers PW. Functional derivative of noninteracting kinetic energy density functional. *Phys Rev A* 2004, 70:022501.
108. Wesolowski TA. Comment on "Accurate frozen-density embedding potentials as a first step towards a subsystem description of covalent bonds" [J. Chem. Phys. 132, 164101 (2010)]. *J Chem Phys* 2011, 135:027101.
109. Fux S, Jacob Ch R, Neugebauer J, Visscher L, Reiher M. Response to "Comment on: 'Accurate frozen-density embedding potentials as a first step towards a subsystem description of covalent bonds' ". *J Chem Phys* 2011, 135:027102.
110. Savin A, Wesolowski TA. Orbital-free embedding effective potential in analytically solvable cases. In: Piecuch P, Maruani J, Delgado-Barrio G, Wilson S, eds. *Advances in the Theory of Atomic and Molecular Systems*. Dordrecht: Springer; 2009, 311–326.
111. de Silva P, Wesolowski TA. Exact non-additive kinetic potentials in realistic chemical systems. *J Chem Phys* 2012, 137:094110.
112. de Silva P, Wesolowski TA. Pure-state noninteracting v-representability of electron densities from Kohn-Sham calculations with finite basis sets. *Phys Rev A* 2012, 85:032518.
113. Jacob Ch R, Visscher L. Density–functional theory approach for the quantum chemical treatment of proteins. *J Chem Phys* 2008, 128:155102.
114. Kiewisch K, Jacob Ch R, Visscher L. Quantum-Chemical Electron Densities of Proteins and of Selected Protein Sites from Subsystem Density Functional Theory. *J Chem Theory Comput* 2013, 9:2425–2440.
115. Zhao Q, Morrison RC, Parr RG. From electron densities to Kohn-Sham kinetic energies, orbital energies, exchange-correlation potentials, and exchange-correlation energies. *Phys Rev A* 1994, 50:2138–2142.

116. van Leeuwen R, Baerends EJ. An exchange–correlation potential with correct asymptotic behaviour. *Phys Rev A* 1994, 49:2421–2431.
117. Kadantsev ES, Stott MJ. Variational method for inverting the Kohn-Sham procedure. *Phys Rev A* 2004, 69:012502.
118. Wang Y, Parr RG. Construction of exact Kohn-Sham orbitals from a given electron density. *Phys Rev A* 1993, 47:R1591.
119. Colonna F, Savin A. Correlation energies for some two- and four-electron systems along the adiabatic connection in density functional theory. *J Chem Phys* 1999, 110:2828.
120. Goodpaster JD, Barnes TA, Miller TF. Embedded density functional theory for covalently bonded and strongly interacting subsystems. *J Chem Phys* 2011, 134:164108.
121. Yang W, Wu Q. Direct Method for Optimized Effective Potentials in Density-Functional Theory. *Phys Rev Lett* 2002, 89:143002.
122. Wu Q, Yang W. A direct optimization method for calculating density functionals and exchange–correlation potentials from electron densities. *J Chem Phys* 2003, 118:2498–2509.
123. Hirata S, Ivanov S, Grabowski I, Bartlett RJ, Burke K, Talman JD. Can optimized effective potentials be determined uniquely? *J Chem Phys* 2001, 115:1635–1649.
124. Staroverov VN, Scuseria GE, Davidson ER. Optimized effective potentials yielding Hartree–Fock energies and densities. *J Chem Phys* 2006, 124:141103.
125. Görling A, Heßelmann A, Jones M, Levy M. Relation between exchange-only optimized potential and Kohn–Sham methods with finite basis sets, and effect of linearly depe ndent products of orbital basis functions. *J Chem Phys* 2008, 128:104104.
126. Heßelmann A, Götz AW, Della Sala F, Görling A. Numerically stable optimized effective potential method with balanced Gaussian basis sets. *J Chem Phys* 2007, 127:054102.
127. Kollmar C, Filatov M. Optimized effective potential method: Is it possible to obtain an accurate representation of the response function for finite orbital basi s sets? *J Chem Phys* 2007, 127:114104.
128. Heaton-Burgess T, Bulat FA, Yang W. Optimized Effective Potentials in Finite Basis Sets. *Phys Rev Lett* 2007, 98:256401.
129. Heaton-Burgess T, Yang W. Optimized effective potentials from arbitrary basis sets. *J Chem Phys* 2008, 129:194102.
130. King RA, Handy NC. Kinetic energy functionals from the Kohn-Sham potential. *Phys Chem Chem Phys* 2000, 2:5049–5056.
131. Jacob Ch R. Unambiguous optimization of effective potentials in finite basis sets. *J Chem Phys* 2011, 135:244102.
132. Boguslawski K, Jacob Ch R, Reiher M. Optimized unrestricted Kohn–Sham potentials from ab initio spin densities. *J Chem Phys* 2013, 138:044111–044111–16.
133. Grimme S. Density functional theory with London dispersion corrections. *WIREs Comput Mol Sci* 2011, 1:211–228.
134. Beyhan SM, Götz AW, Visscher L. Bond energy decomposition analysis for subsystem density functional theory. *J Chem Phys* 2013, 138:094113.
135. Wesolowski TA, Ellinger Y, Weber J. Density functional theory with an approximate kinetic energy functional applied to study structure and stability of weak van der Waals complexes. *J Chem Phys* 1998, 108:6078.
136. Tran F, Weber J, Wesolowski TA. Theoretical Study of the Benzene Dimer by the Density-Functional-Theory Formalism Based on Electron-Density Partitioning. *Helv Chim Acta* 2001, 84:1489–1503.
137. Tran F, Weber J, Wesolowski TA. Physisorption of Molecular Hydrogen on Polycyclic Aromatic Hydrocarbons: A Theoretical Study. *J Phys Chem B* 2002, 106:8689–8696.
138. Tran F, Alameddinee B, Jenny TA, Wesolowski TA. π-Stacking Behavior of Selected Nitrogen-Containing PAHs. *J Phys Chem A* 2004, 108:9155–9160.
139. Leopoldini M, Russo N, Toscano M, Dulak M, Wesolowski TA. Mechanism of Nitrate Reduction by *Desulfovibrio desulfuricans* Nitrate Reductase—A Theoretical Investigation. *Chem Eur J* 2006, 12:2532–2541.
140. Zhao Y, Truhlar DG. Design of Density Functionals That Are Broadly Accurate for Thermochemistry, Thermochemical Kinetics, and Nonbonded Interactions. *J Phys Chem A* 2005, 109:5656–5667.
141. Zhao Y, Truhlar DG. How well can new-generation density functional methods describe stacking interactions in biological systems? *Phys Chem Chem Phys* 2005, 7:2701–2705.
142. Kevorkyants R, Dulak M, Wesolowski TA. Interaction energies in hydrogen-bonded systems: A testing ground for subsystem formulation of density-functional theory. *J Chem Phys* 2006, 124:024104.
143. Götz AW, Beyhan SM, Visscher L. Performance of Kinetic Energy Functionals for Interaction Energies in a Subsystem Formulation of Density Functional Theory. *J Chem Theory Comput* 2009, 5:3161–3174.
144. Hong G, Strajbl M, Wesolowski T, Warshel A. Constraining the Electron Densities in DFT Method as an Effective Way for *Ab Initio* Studies of Metal-Catalyzed Reactions. *J Comput Chem* 2000, 21:1554–1561.
145. Štrajbl M, Hong G, Warshel A. Ab Initio QM/MM Simulation with Proper Sampling: "First Principle" Calculations of the Free Energy of the Autodissociation of Water in Aqueous Solution. *J Phys Chem B* 2002, 106:13333–13343.

146. Olsson MHM, Hong G, Warshel A. Frozen Density Functional Free Energy Simulations of Redox Proteins: Computational Studies of the Reduction Potential of Plastocyanin and Rusticyanin. *J Am Chem Soc* 2003, 125:5025–5039.
147. Trail JR, Bird DM. Density-functional embedding using a plane-wave basis. *Phys Rev B* 2000, 62:16402–16411.
148. Mehl MJ, Stokes HT, Boyer LL. Development of a Kohn–Sham like Potential in the Self-Consistent Atomic Deformation Model. *J Phys Chem Solids* 1996, 57:1405–1407.
149. Stokes HT, Boyer LL, Mehl MJ. Spherical self-consistent atomic deformation model for first-principles energy calculations in ionic crystalline solids. *Phys Rev B* 1996, 54:7729–7736.
150. Boyer LL, Stokes HT, Mehl MJ. Application of a Kohn–Sham-like Formulation of the Self-Consistent Atomic Deformation Model. *Ferroelectrics* 1997, 194:173–186.
151. Boyer LL, Stokes HT, Mehl MJ. Calculation of Polarization Using a Density Functional Method with Localized Charge. *Phys Rev Lett* 2000, 84:709–712.
152. Ossowski MM, Boyer LL, Mehl MJ, Stokes HT. Lattice dynamics and elastic properties of corundum by the self-consistent atomic deformation method. *Phys Rev B* 2002, 66:224302.
153. Boyer LL, Stokes HT, Ossowski MM, Mehl MJ. Self-consistent atomic deformation method for application of density functional theory. *Phys Rev B* 2008, 78:045121.
154. Zhang X, Lu G. Quantum mechanics/molecular mechanics methodology for metals based on orbital-free density functional theory. *Phys Rev B* 2007, 76:245111.
155. Zhang X, Wang C-Y, Lu G. Electronic structure analysis of self-consistent embedding theory for quantum/molecular mechanics simulations. *Phys Rev B* 2008, 78:235119.
156. Zhang X, Lu G, Curtin WA. Multiscale quantum/atomistic coupling using constrained density functional theory. *Phys Rev B* 2013, 87:054113.
157. Hong G, Rosta E, Warshel A. Using the constrained DFT Approach in Generating Diabatic Surfaces and Off Diagonal Empirical Valence Bond Terms for Modeling Reactions in Condensed Phases. *J Phys Chem B* 2006, 110:19570–19574.
158. Xiang Y, Warshel A. Quantifying Free Energy Profiles of Proton Transfer Reactions in Solution and Proteins by Using a Diabatic FDFT Method. *J Phys Chem B* 2008, 112:1007–1015.
159. Kamerlin SCL, Warshel A. The empirical valence bond model: theory and applications. *WIREs Comp Mol Sci* 2011, 1:30–45.
160. Kaduk B, Kowalczyk T, Voorhis TV. Constrained Density Functional Theory. *Chem Rev* 2012, 112:321–370.
161. Pavanello M, Neugebauer J. Modelling charge transfer reactions with the Frozen Density Embedding formalism. *J Chem Phys* 2011, 135:234103.
162. Pavanello M, Voorhis TV, Visscher L, Neugebauer J. An accurate and linear-scaling method for calculating charge-transfer energies and diabatic couplings. *J Chem Phys* 2013, 138:054101.
163. Reichardt C, Welton T. *Solvents and Solvent Effects in Organic Chemistry*. Weinheim: Wiley-VCH; 2011.
164. Bader R. *Atoms in Molecules*. Oxford: Clarendon Press; 1990.
165. García-Lastra JM, Wesolowski TA, Barriuso MT, Aramburu JA, Moreno M. Optical and vibrational properties of MnF_6^{4-} complexes in cubic fluoroperovskites: insight through embedding calculations using Kohn-Sham equations with constrained electron density. *J Phys: Condens Matter* 2006, 18:1519–1534.
166. Salahub DR, Goursot A, Weber J, Köster AM. Applied density functional theory and the deMon codes 1964–2004. In: Dykstra CE, Frenking G, Kim KS, Scuseria GE, eds. *Theory and Applications of Computational Chemistry: The First Forty Years*. Amsterdam: Elsevier; 2005, 1079–1097.
167. Wesolowski TA, Goursot A, Weber J. Properties of CO adsorbed in ZSM5 zeolite: Density functional theory study using the embedding scheme based on electron density partitioning. *J Chem Phys* 2001, 115:4791.
168. Dułak M, Kamiński JW, Wesołowski TA. Equilibrium Geometries of Noncovalently Bound Intermolecular Complexes Derived from Subsystem Formulation of Density Functional Theory. *J Chem Theory Comput* 2007, 3:735–745.
169. Iannuzzi M, Kirchner B, Hutter J. Density functional embedding for molecular systems. *Chem Phys Lett* 2006, 421:16–20.
170. Hodak M, Lu W, Bernholc J. Hybrid *ab initio* Kohn–Sham density functional theory/frozen-density orbital-free density functional theory simulation method suitable for biological systems. *J Chem Phys* 2008, 128:014101.
171. Shimojo F, Kalia RK, Nakano A, Vashishta P. Embedded divide-and-conquer algorithm on hierarchical real-space grids: parallel molecular dynamics simulation based on linear-scaling density functional theory. *Comput Phys Commun* 2005, 167:151–164.
172. Vashishta P, Kalia RK, Nakano A, Homan BE, McNesby KL. Multimillion Atom Reactive Simulations of Nanostructured Energetic Materials. *J Propul Power* 2007, 23:688–692.

173. Jacob Ch R, Visscher L. Calculation of nuclear magnetic resonance shieldings using frozen-density embedding. *J Chem Phys* 2006, 125:194104.
174. Bulo RE, Jacob Ch R, Visscher L. NMR Solvent Shifts of Acetonitrile from Frozen Density Embedding Calculations. *J Phys Chem A* 2008, 112:2640–2647.
175. Wesolowski TA. Application of the DFT-based embedding scheme using an explicit functional of the kinetic energy to determine the spin density of Mg^+ embedded in Ne and Ar matrices. *Chem Phys Lett* 1999, 311:87–92.
176. Neugebauer J, Louwerse MJ, Belanzoni P, Wesolowski TA, Baerends EJ. Modeling solvent effects on electron spin resonance hyperfine couplings by frozen-density embedding. *J Chem Phys* 2005, 123:114101.
177. Fradelos G, Wesolowski TA. Importance of Going beyond Coulombic Potential in Embedding Calculations for Molecular Properties: The Case of Iso-G for Biliverdin in Protein-Like Environment. *J Chem Theory Comput* 2011, 7:213–222.
178. Fleming GR, Martin JL, Breton J. Rates of primary electron transfer in photosynthetic reaction centres and their mechanistic implications. *Nature* 1988, 333:190.
179. Kirmaier C, Holten D, Parson W. Temperature and detection-wavelength dependence of the picosecond electron-transfer kinetics measured in Rhodopseudomonas sphaeroides reactions centers. Resolution of new spectral and kinetic components in the primary charge-separation process. *Biochim Biophys Acta* 1985, 810:49–61.
180. Collins AM, Kirmaier C, Holten D, Blankenship RE. Kinetics and energetics of electron transfer in reaction centers of the photosynthetic bacterium Roseiflexus castenholzii. *Biochim Biophys Acta* 2011, 1807:262.
181. Zbiri M, Atanasov M, Daul C, Garcia-Lastra JM, Wesolowski TA. Application of the density functional theory derived orbital-free embedding potential to calculate the splitting energies of lanthanide cations in chloroelpasolite crystals. *Chem Phys Lett* 2004, 397:441–446.
182. Zbiri M, Daul C, Wesolowski TA. Effect of the f-Orbital Delocalization on the Ligand-Field Splitting Energies in Lanthanide-Containing Elpasolites. *J Chem Theory Comput* 2006, 2:1106–1111.
183. Atanasov M, Daul C, Güdel HU, Wesolowski TA, Zbiri M. Ground States, Excited States, and Metal–Ligand Bonding in Rare Earth Hexachloro Complexes: A DFT-Based Ligand Field Study. *Inorg Chem* 2005, 44:2954–2963.
184. Casida ME, Wesolowski TA. Generalization of the Kohn–Sham Equations with Constrained Electron Density Formalism and Its Time-Dependent Response Theory Formulation. *Int J Quantum Chem* 2004, 96:577–588.
185. Casida ME. Time-dependent density functional response theory for molecules. In: Chong DP, ed. *Recent Advances in Density Functional Methods Part I*. Singapore: World Scientific; 1995, 155–192.
186. van Gisbergen SJA, Snijders JG, Baerends EJ. Implementation of time-dependent density functional response equations. *Comput Phys Commun* 1999, 118:119–138.
187. Marques MAL, Gross EKU. Time-dependent density-functional theory. In: Fiolhais C, Nogueira F, Marques M, eds. *A Primer in Density Functional Theory*. Berlin: Springer; 2003, 144–184.
188. Rosa A, Ricciardi G, Gritsenko OV, Baerends EJ. Excitation energies of metal complexes with time-dependent density functional theory. *Struct Bonding* 2004, 112:49–116.
189. Marques MAL, Gross EKU. Time-Dependent Density Functional Theory. *Annu Rev Phys Chem* 2004, 55:427–455.
190. Dreuw A, Head-Gordon M. Single-Reference ab Initio Methods for the Calculation of Excited States of Large Molecules. *Chem Rev* 2005, 105:4009–4037.
191. Wesolowski TA. Hydrogen-bonding induced shifts of the excitation energies in nucleic acid bases: an interplay between electrostatic and electron density overlap effects. *J Am Chem Soc* 2004, 126:11444–11445.
192. Neugebauer J. Couplings between electronic transitions in a subsystem formulation of time-dependent density functional theory. *J Chem Phys* 2007, 126:134116.
193. Fradelos G, Kaminski JW, Wesołowski TA, Leutwyler S. Cooperative Effect of Hydrogen-Bonded Chains in the Environment of a $\pi \rightarrow \pi^*$ Chromophore. *J Phys Chem A* 2009, 113:9766–9771.
194. Neugebauer J. Photophysical Properties of Natural Light-Harvesting Complexes Studied by Subsystem Density Functional Theory. *J Phys Chem B* 2008, 112:2207–2217.
195. König C, Schlüter N, Neugebauer J. Direct determination of exciton couplings from subsystem time-dependent density-functional theory within the tamm–dancoff approximation. *J Chem Phys* 2013, 138:034104.
196. Pavanello M. On the subsystem formulation of linear-response time-dependent DFT. *J Chem Phys* 2013, 138:204118.
197. Neugebauer J. Orbital-free embedding calculations of electronic spectra. In: Wesolowski TA, Wang YA, eds. *Recent Progress in Orbital-Free Density Functional Theory*. Singapore: World Scientific; 2013, 325–356.
198. Neugebauer J, Louwerse MJ, Baerends EJ, Wesolowski TA. The merits of the frozen-density embedding scheme to model solvatochromic shifts. *J Chem Phys* 2005, 122:094115.

199. Neugebauer J, Jacob Ch R, Wesolowski TA, Baerends EJ. An Explicit Quantum Chemical Method for Modeling Large Solvation Shells Applied to Aminocoumarin C151. *J Phys Chem A* 2005, 109:7805–7814.
200. Zhou X, Wesolowski TA, Tabacchi G, Fois E, Calzaferri G, Devaux A. First-principles simulation of the absorption bands of fluorenone in zeolite L. *Phys Chem Chem Phys* 2013, 15:159–167.
201. Kovyrshin A, Neugebauer J. Potential-Energy Surfaces of Local Excited States from Subsystem- and Selective Kohn-Sham-TDDFT. *Chem Phys* 2011, 391:147–156.
202. Neugebauer J, Baerends EJ. Exploring the Ability of Frozen-Density Embedding to Model Induced Circular Dichroism. *J Phys Chem A* 2006, 110:8786–8796.
203. Tomasi J, Mennucci B, Cammi R. Quantum Mechanical Continuum Solvation Models. *Chem Rev* 2005, 105:2999–3094.
204. Kovalenko A. Three-dimensional RISM theory for molecular liquids and solid-liquid interfaces. In: Hirata F, ed. *Molecular Theory of Solvation: Understanding Chemical Reactivity*. Dordrecht, The Netherlands: Kluwer; 2003, 169–275.
205. Klamt A, Schüürmann G. COSMO: a new approach to dielectric screening in solvents with explicit expressions for the screening energy and its gradient. *J Chem Soc, Perkin Trans* 1993, 2:799–805.
206. Zhou X, Kaminski JW, Wesołowski TA. Multiscale modelling of solvatochromic shifts from frozen-density embedding theory with non-uniform continuum model of the solvent: the coumarin 153 case. *Phys Chem Chem Phys* 2011, 13:10565–10576.
207. Fradelos G, Lutz JJ, Wesołowski TA, Piecuch P, Włoch M. Shifts in excitation energies induced by hydrogen bonding: a comparison of the embedding and supermolecular time-dependent density functional theory calculations with the equation-of-motion coupled-cluster results. In: Hoggan PE, Brändas EJ, Maruani J, Piecuch P, Delgado-Barrio G, eds. *Advances in the Theory of Quantum Systems in Chemistry and Physics, vol 22 of Progress in Theoretical Chemistry and Physics*. Dordrecht: Springer; 2012, 219–248.
208. König C, Neugebauer J. First-principles calculations of electronic spectra of light-harvesting complex II. *Phys Chem Chem Phys* 2011, 13:10475–10490.
209. König C, Neugebauer J. Protein effects on the optical spectrum of the fenna–matthews–olson complex from fully quantum chemical calculations. *J Chem Theory Comput* 2013, 9:1808–1820.
210. Neugebauer J, Veldstra J, Buda F. Theoretical Spectroscopy of Astaxanthin in Crustacyanin Proteins: Absorption, Circular Dichroism, and Nuclear Magnetic Resonance. *J Phys Chem B* 2011, 115:3216–3225.
211. Neugebauer J, Curutchet C, Munos-Losa A, Mennucci B. A Subsystem TDDFT Approach for Solvent Screening Effects on Excitation Energy Transfer Couplings. *J Chem Theory Comput* 2010, 6:1843–1851.
212. König C, Neugebauer J. Exciton coupling mechanisms analyzed with subsystem tddft: Direct vs. pseudo exchange effects. *J Phys Chem B* 2013, 117:3480–3487.
213. Neugebauer J. On the calculation of general response properties in subsystem density functional theory. *J Chem Phys* 2009, 131:084104.
214. Mukhopadhyay P, Zuber G, Wipf P, Beratan DN. Contribution of a solute's chiral solvent imprint to optical rotation. *Angew Chem, Int Ed* 2007, 46:6450–6452.
215. Neugebauer J. Induced Chirality in Achiral Media — How Theory Unravels Mysterious Solvent Effects. *Angew Chem, Int Ed* 2007, 46:7738–7740.
216. Huang P, Carter EA. Advances in Correlated Electronic Structure for Solids, Surfaces, and Nanostructures. *Annu Rev Phys Chem* 2008, 59:261–290.
217. Gomes ASP, Jacob Ch R. Quantum-chemical embedding methods for treating local electronic excitations in complex chemical systems. *Annu Rep Prog Chem C* 2012, 108:222.
218. Govind N, Wang YA, da Silva AJR, Carter EA. Accurate ab initio energetics of extended systems via explicit correlation embedded in a density functional environment. *Chem Phys Lett* 1998, 295:129–134.
219. Govind N, Wang YA, Carter EA. Electronic-structure calculations by first-principles density-based embedding of explicitly correlated systems. *J Chem Phys* 1999, 110:7677–7688.
220. Aquilante F, Wesolowski TA. Self-consistency in frozen-density embedding theory based calculations. *J Chem Phys* 2011, 135:084120.
221. Klüner T, Govind N, Wang YA, Carter EA. Prediction of electronic excited states of adsorbates on metal surfaces from first principles. *Phys Rev Lett* 2001, 86:5954–5957.
222. Klüner T, Govind N, Wang YA, Carter EA. Periodic density functional embedding theory for complete active space self-consistent field and configuration interaction calculations: Ground and excited states. *J Chem Phys* 2002, 116:42–54.
223. Huang P, Carter EA. Self-consistent embedding theory for locally correlated configuration interaction wave functions in condensed matter. *J Chem Phys* 2006, 125:084102.
224. Lahav D, Klüner T. A self-consistent density based embedding scheme applied to the adsorption of CO on Pd(111). *J Phys: Condens Matter* 2007, 19:226001.
225. Huang C, Carter EA. Embedding theory for excited states. *J Chem Phys* 2011, 135:194104.

226. Khait YG, Hoffmann MR. Embedding theory for excited states. *J Chem Phys* 2010, 133:044107.
227. Höfener S, Gomes ASP, Visscher L. Molecular properties via a subsystem density functional theory formulation: A common framework for electronic embedding. *J Chem Phys* 2012, 136:044104.
228. Christiansen O, Jørgensen P, Hättig C. Response functions from Fourier component variational perturbation theory applied to a time-averaged quasienergy. *Int J Quantum Chem* 1998, 68:1–52.
229. Kanan DK, Sharifzadeh S, Carter EA. Quantum mechanical modeling of electronic excitations in metal oxides: Magnesia as a prototype. *Chem Phys Lett* 2012, 519-520:18–24.
230. Gomes ASP, Jacob Ch R, Visscher L. Calculation of local excitations in large systems by embedding wave-function theory in density-functional theory. *Phys Chem Chem Phys* 2008, 10:5353–5362.
231. Daday C, König C, Valsson O, Neugebauer J, Filippi C. State-Specific Embedding Potentials for Excitation-Energy Calculations. *J Chem Theory Comput* 2013, 9:2355–2367.
232. Höfener S, Visscher L. Calculation of electronic excitations using wave-function in wave-function frozen-density embedding. *J Chem Phys* 2012, 137:204120.
233. Roncero O, de Lara-Castells MP, Villarreal P, Flores F, Ortega J, Paniagua M, Aguado A. An inversion technique for the calculation of embedding potentials. *J Chem Phys* 2008, 129:184104.
234. Roncero O, Zanchet A, Villarreal P, Aguado A. A density-division embedding potential inversion technique. *J Chem Phys* 2009, 131:234110.
235. Goodpaster JD, Barnes TA, Manby FR, Miller TF. Density functional theory embedding for correlated wavefunctions: Improved methods for open-shell systems and transition metal complexes. *J Chem Phys* 2012, 137:224113.
236. Svensson M, Humbel S, Froese RDJ, Matsubara T, Sieber S, Morokuma K. ONIOM: A Multilayered Integrated MO + MM Method for Geometry Optimizations and Single Point Energy Predictions. A Test for Diels–Alder Reactions and $Pt(P(t\text{-}Bu)_3)_2 + H_2$ Oxidative Addition. *J Phys Chem* 1996, 100:19357–19363.
237. Kitaura K, Ikeo E, Asada T, Nakano T, Uebayasi M. Fragment molecular orbital method: an approximate computational method for large molecules. *Chem Phys Lett* 1999, 313:701–706.
238. Fedorov DG, Kitaura K. Extending the Power of Quantum Chemistry to Large Systems with the Fragment Molecular Orbital Method. *J Phys Chem A* 2007, 111:6904–6914.

